From the Electromagnetic Pulse to High-Power Electromagnetics

CARL E. BAUM, FELLOW, IEEE

Invited Paper

Since the 1960's significant effort has gone into developing requisite technology for the nuclear electromagnetic pulse (EMP). In the late 1970's several important summary documents were published. This paper updates this information to the present. EMP has impacted a set of related areas which we can collectively refer to as high-power electromagnetics (HPE). This also includes direct-strike lightning, high-power microwaves (HPM), and some aspects of transient radar.

I. Introduction

Electromagnetic pulse (EMP) technology has spread to most major industrialized countries on the globe. (This has other initials in other languages, e.g., IEM in French and ЭМИ in Russian.) The EMP generated by a high altitude nuclear detonation can cover a continent exposing communications and other electronic equipment to a potentially damaging or functionally disrupting environment. So while other forms of EMP (e.g., surface burst, system-generated EMP (SGEMP) associated with γ and X rays incident on exoatmospheric systems) are also important the high-altitude EMP (or HEMP) was recognized since the early 1960's as the most significant [115].

The reader may have already heard of EMP in a more popular context. Articles (e.g., [138]) and even a paperback book [182] have appeared for nonspecialists (in either electromagnetics or nuclear physics). Newspaper articles have appeared in numerous languages. Television news programs have often presented it. At least one full TV program has been devoted to it (in German) [187]. Even 007 has had to deal with it on a few occasions.

If one were building an EMP library sufficient room should be allowed. The notes on EMP and related subjects which the author edited occupy two full six-shelf bookcases (over 1600 Notes at last count). By now many of these papers have appeared in various traditional journals or have been incorporated into books. On a more modest scale there are some books, review papers, and journal special issues concerned with EMP and related subjects [1]–[21]. One can also find a summary of the nuclear EMP in [22] and information concerning component effects (which will not be emphasized here) in [23].

As summarized in Table 1, EMP history begins in 1945 with the first nuclear event. In a recently uncovered historical footnote, J. L. Malik of Los Alamos Scientific Laboratory (LASL), NM, has conveyed some interesting information to EMP archaeologist C. N. Vittitoe of Sandia Laboratories, NM. It seems that a LASL notebook of F. Reines found in the files of R. E. Partridge records that in the fall of 1951, C. H. Papas (later of Cal Tech) suggested the Compton current as the EMP source.

The history is continued in Table 2. Since the mid-1970's EMP technology has been extended and has spawned some related areas. The concepts for EMP interaction and hardening are directly applicable in the case of high-power microwave and lightning environments. The transient (broadband) electromagnetic sensors and measurement techniques apply to all kinds of big, fast electromagnetic fields, currents, voltages, etc. The pulse power involves similar fast Marx generators. The radiation of big fast electromagnetic pulses as done by EMP simulators is a similar problem in antennas (and perhaps switching and pulse power) for transient radars. The physics (especially air chemistry) of the EMP source region is similar to that of the lightning arc and corona. In recent years this common set of technologies has come to be identified as high-power electromagnetics (HPE) [166]. There is an international working group of Commission E of International Radio Scientific Union (URSI) with this title, currently chaired by R. L. Gardner. Sessions at conferences have been organized on this subject for several years now. So in this paper in appropriate sections the common technologies are grouped together.

It is hard to be precise as to when one should break the history between the old and new eras since the broadening of the EMP technology to the related areas (HPE) was a gradual process. However, one can identify a few events in the late 1970's (the first few items in Table 2) as significant in this regard. From the early 1970's EMP technology began to appear in the professional conferences (IEEE An-

Manuscript received July 22, 1991; revised December 16, 1991.
The author is with Phillips Laboratory (AFSC), Kirtland, AFB, NM 87117.
IEEE Log Number 9201320.

Table 1 Important Events in the History of EMP (from [3])

1945	TRINITY EVENT; electronic equipment shielded reportedly because of Fermi's expectations of EM signals from a nuclear burst.
1951–1952	First deliberate EMP observations made by Shuster, Cowan, and Reines.
1952–1953	First British atomic tests; instrumentation failures attributed to "radioflash."
1954	Garwin of LASL proposes prompt gamma-produced Compton currents as primary sources of EMP.
1957	Bethe makes estimate of high-altitude EMP signals using electric dipole model (early-time peak incorrect).
1957	Haas makes magnetic field measurements for PLOMBBOB test series (interest in EMP possibly setting off magnetic mines).
1958	Joint British/U.S. meeting begins discussions of system EMP vulnerability and hardness issues.
1958	Kampaneets (USSR) publishes open literature paper on EMP from atomic explosion.
1959	Pomham and Taylor of the U.K. present a theory of "radioflash."
1959	First interest in EMP coupling to underground cables of Minuteman missile.
1962	FISHBOWL high-altitude tests; EMP measurements driven off scale; first-indications of the magnitude of high-altitude EMP signal.
1962	SMALL BOY ground burst EMP test.
1962	Karzas and Latter publish two open literature papers on using EMP signals for detections of nuclear tests; bomb case EMP and hydromagnetic EMP considered.
1963	Open literature calls for EMP hardening of military systems begin to appear.
1963–1964	First EMP system tests carried out by Air Force Weapons Laboratory (AFWL) (now Phillips Laboratory).
1963–1964	Longmire gives a series of EMP lectures at AFWL; presents detailed theory of ground burst EMP and shows that the peak of the high-altitude EMP signals is explained by magnetic field turning (magnetic dipole signal).
1964	First note in the LASL/AFWL EMP notes series published.
1965	Karzas and Latter publish first open literature paper giving high-frequency approximation for the high-altitude magntic diople signal.
1967	Construction of ALECS as the first guided-wave simulator is completed for EMP simulation on missiles.
1967	AJAX underground nuclear test.
1969	Close-in EMP mechanisms recognized and evaluated by Graham and Schaefer.
1970	EMP underground test feasibility recognized and preliminary design presented by Schaefer.
1973	First joint neclear EMP meeting at AFWL.
1974	MING BLADE underground EMP test for confirmation of near surface burst EMP models.
1975	DINING CAR underground EMP test as the first system hardware EMP test.
1975	MIGHTY EPIC underground EMP test.

Table 2 Important Events in the History of HPE

1976	*Transient Electromagnetc Fields* book (L. B. Felsen (Ed.)), and PROCEEDINGS OF THE IEEE review paper on same subject (C. E. Baum) (includes first reviews on singularity expansion method (SEM)).
1978	Special Joint Issue on the Nuclear Electromagnectic Pulse, IEEE TRANSACTIONS ON ANTENNAS AND PROPAGATION and IEEE TRANSACTIONS ON ELECTROMAGNETIC COMPATIBILITY.
1978	First public Nuclear EMP meeting (NEM) followed by NEM's in even numbered years.
1978	Lightning-channel physics and direct-strike interaction program begins at Langmuir Observatory, NM, involving N.M. Tech, AFWL, AF Flight Dynamics Lab, and French.
1979	Major EMP simulators beginning with SIEM II (in France) are constructed in Europe.
1980	ATLAS I EMP simulator completed (for large aircraft on wooden trestle test stand).
1980	*EMP Interaction* book (K. S. H. Lee (Ed.)), first published by AFWL.
1980	Lightning strikes to NASA F-106 begun, later joined by CV-580 and French Transall.
1981	Special Issue on the Singularity Expansion Method, Electromagnetics.
1981	Formation of URSI Commission E International Working Group: Scientific Basis for Noise and Interference Control (C. E. Baum, Chairman).
1982	Special Issue on Lightning and Its Interaction with Aircraft, IEEE TRANSACTIONS ON ELECTROMAGNETIC COMPATIBILITY.
1983	First EMP Interaction and Hardening (EMP 201) short course (Socorro, NM).
1984	URSI statement: Nuclear electromagnetic pulse (EMP) and associated effects (concerned with civil communications and electrical power).
1985	(First) Special Issue of High-Power Microwave Generation, IEEE TRANSACTIONS ON PLASMA SCIENCE.
1986	Special Issue of Electromagnetic Topology of Large Systems, Electromagnetics.
1987	Public HEMP waveforms (C. L. Longmire *et al.*).
1987	First High-Power Electromagnetic Special Session, National Radio Science Meeting (USNC/URSI).
1987	*High-Power Microwave Sources* book (V. L. Granatstein and I. Alexeff (Eds.)).
1988	EMPRESS II EMP simulator completed (on ocean-going barge for testing ships).
1990	*Lightning Electromagnetics* book (R. L. Gardner (Ed.)).
1990	Formation of URSI Commission E International Working Group: High-Power Electromagnetics (R. L. Gardner, Chairman).
(In Progress)	Special Issue on High-Power Microwaves, IEEE TRANSACTIONS ON ELECTROMAGNETIC COMPATIBILITY.

tennas and Propagation and Electromagnetic Compatibility Societies, and URSI) in a big way associated with general transient electromagnetics, particularly as associated with the singularity expansion method (SEM) (summarized in [2], [4]). Then in 1978 EMP effectively "went public" with the public symposia, the Nuclear EMP Meetings (NEM's) in cooperation with the professional societies, and with the EMP Special Issue. Combined with the EMP Interaction book [3] in 1980, this gives an appropriate time mark in the history. Of course, one sees this better with the benefit of hindsight. Noting that the EMP Special Issue was published in 1978, the editorial board of the PROCEEDINGS OF THE IEEE felt that it was time to have a review updating the subject: the present paper. Some additional history is contained in [145].

In organizing this paper, including every reference hav-

ing something to do with the subject would have been impractical. Referring to the cited notes, articles, conference proceedings, etc., the reader will easily come across many more titles. Here the author has tried to include the major references and those needed to fill out the story on major portions of the technology. For example, in Section V (interaction) the author has concentrated on the "big picture", i.e., interaction with the system as a whole (or major portions thereof) and controlling the same. This leaves out the plethora of papers concerning the individual pieces (apertures, antennas, cavities, cable shields, etc.) as well as the response of individual circuit elements (upset, burnout, etc.) the latter being treated in [23] as well as many articles in IEEE TRANSACTIONS ON NUCLEAR SCIENCE. There are various other fields (such as techniques for numerical computations) which are useful in many fields (including the present one) which are not treated here.

II. ENVIRONMENTS

There is much known about the various HPE environments. Here we briefly summarize some important aspects. For later use we have

$$\begin{aligned} Z_0 &= \sqrt{\frac{\mu_0}{\epsilon_0}} \equiv \text{ wave impedance of free space} \\ c &= \frac{1}{\sqrt{\mu_0 \epsilon_0}} \equiv \text{ speed of light} \\ s &= \Omega + jw \equiv \text{ complex frequency or Laplace transform variable} \\ \tilde{f}(s) &= \int_{-\infty}^{\infty} f(t) e^{-st}\, dt \equiv \text{ two-sided Laplace transform} \end{aligned} \tag{2.1}$$

with the Bromwich contour the strip of convergence in the s plane.

A. HEMP

The basic theory of the high-altitude EMP (the KLL or Karzas–Latter–Longmire model) is summarized in [1(Longmire, pp. 3–14)] and [3]. The basic equation for the generation of the transverse electric field reads

$$\left[2\frac{\partial}{\partial r} + Z_0\sigma\right]\vec{E}_t = -Z_0\vec{J}_{c_t} \tag{2.2}$$

where r is the radial coordinate and the parameters are taken as functions of r and retarded time $t - r/c$. This is a high-frequency or outward-going wave approximation in which for constant retarded time changes with respect to r are relatively small. The Compton current density $\vec{J}_c$ is initially associated with γ rays stripping electrons from air molecules and sending them initially in the r direction (in an average sense). By collisions with the air molecules these electrons are slowed down with a range of about a meter at sea level, but of about 100 m to 1 km at the 20–40 km altitude characteristic of the HEMP source region. In (2.2) we have the transverse (to r) Compton current density which arises from the interaction (turning) of the Compton electrons in the Earth's magnetic field. The transverse Compton current density $\vec{J}_{c_t}$ reaches its maximum value when the turning radius of the average Compton electron is comparable to its range.

The air conductivity σ is associated with the low-energy electrons produced by the collision of the Compton electrons with air molecules. The mobility is a strong function of the electric field. Conduction electrons are lost by attachment to oxygen (attachment time 10^{-8} s at sea level, but much slower at high altitude) and more are produced by avalanche due to the high fields, especially at high altitude. Noting that the source currents and air conductivity increase together during the early portions of the pulse, there is a saturation effect (limiting the electric field) when the conductivity is large enough. From (2.2) in scalar form we have a saturation transverse electric field as

$$E_{t_s} = -\frac{J_{c_t}}{\sigma}. \tag{2.3}$$

A simple calculation using an exponentially rising (10 ns time constant) γ source gives about 6×10^4 V/m for a sufficiently strong source [3].

Recently there have appeared some public HEMP waveforms [84], [173]. These rely on idealized γ-ray waveforms which still give reasonable electromagnetic fields. The calculations include state-of-the-art treatment of the resulting Compton currents and air conductivity. These are summarized in Figs. 1 and 2. Most heights of burst are 400 km, with one at 200 km. The observer ground range is to the south of the burst point with an Earth's magnetic field of 5.6 mT with dip angle of 70° (field lines out of Earth inclined 20° to south from vertical) appropriate to the central U.S. This idealized nuclear device is assumed to produce 10 kT of γ rays with a rise time of *zero* seconds and an exponential decay time of 10 ns, thereby allowing these results to be unclassified (and publicly available). The references give more detail. While these do not encompass every conceivable situation, they are very useful for engineering (interaction, simulation, testing, etc.) purposes.

To summarize these results one can use some simple analytic waveforms [3], [83]. One here used is labeled QEXP and has the form (taken for a single polarization)

$$\begin{aligned} E(t) &= E_1 k_1 \left\{e^{-\alpha_1(t-t_1)} + e^{-\beta_1(t-t_1)}\right\}^{-1} \\ \tilde{E}(s) &= E_1 k_1 \frac{\pi}{\alpha_1 + \beta_1} \csc\left(\pi \frac{s+\beta}{\alpha+\beta}\right) e^{-st_1} \\ \left|\tilde{E}(j\omega)\right| &= E_1 k_1 \frac{\pi}{\alpha_1 + \beta_1} \left[\sinh^2\left(\frac{\pi\omega}{\alpha_1+\beta_1}\right) + \sin^2\left(\frac{\pi\beta_1}{\alpha_1+\beta_1}\right)\right]^{-1/2}. \end{aligned} \tag{2.4}$$

This has the advantage of all time derivatives continuous, but is nonzero for negative time. A time shift parameter t_1 can be used, if desired, to shift the time of waveform peak for convenience. Another simpler waveform labeled DEXP

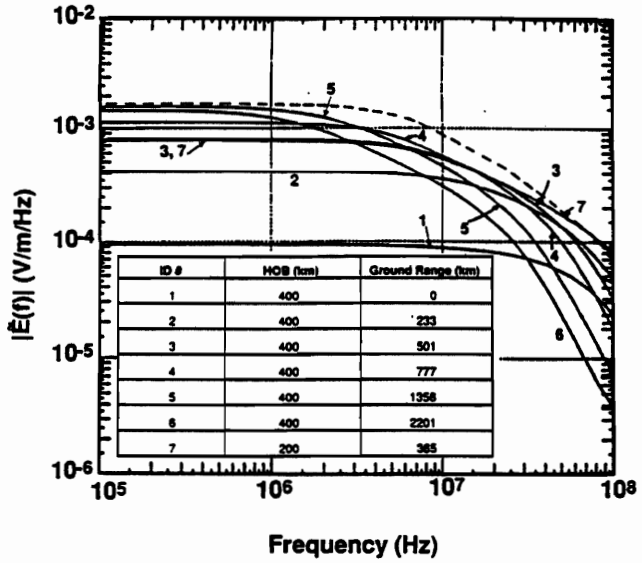

Fig. 1. Comparison of selected HEMP calculations with a frequency domain DEXP curve fit (dashed curve).

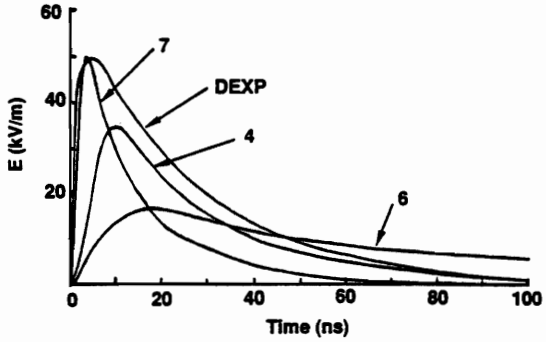

Fig. 2. Comparison of selected HEMP calculations with a time domain DEXP curve fit.

has the form:

$$E(t) = E_2 k_2 \{-e^{-\alpha_2 t} + e^{-\beta_2 t}\} u(t)$$
$$\tilde{E}(s) = E_2 k_2 \left\{ -\frac{1}{s+\alpha_2} + \frac{1}{s+\beta_2} \right\}. \quad (2.5)$$

This has a discontinuous slope at $t = 0$ and is not as good as QEXP for matching the frequency spectrum above about 200 MHz.

One of the uses of these canonical waveforms is for providing appropriate fits and bounds for engineering use. As indicated in Fig. 1 the dashed line gives a bounding spectrum for the entire set of waveforms. This is given by

$$E_1 = E_2 = 50 \text{ kV/m (peak)}$$
$$k_1 = 1.114, \quad k_2 = 1.3$$
$$\tilde{E}(0) = 1.5 \times 10^{-3} (\text{V/m})/\text{Hz}$$
$$= \text{low-frequency content or area under time-domain waveform}$$
$$\alpha_1 = 1.6 \times 10^9 \text{s}^{-1}, \quad \alpha_2 = 6.0 \times 10^8 \text{s}^{-1}$$
$$\beta_1 = 3.7 \times 10^7 \text{s}^{-1}, \quad \beta_2 = 4.0 \times 10^7 \text{s}^{-1} \quad (2.6)$$

The 10%–90% rise time of the QEXP waveform is 2.4 ns while that for the DEXP is 2.6 ns. Over the range 100 kHZ–100 MHz there is no significant difference in the two fits. Figure 2 shows the time-domain form of DEXP. Note that these waveforms are chosen to be a tight bound in frequency domain. As discussed later the interaction process is in general a one characterized by many resonances. In order to have the time-domain strengths of these resonances (damped sinusoids) adequate, it is necessary to have the environment adequate at each of these frequencies. This gives as a necessary condition that a single environmental waveform have its frequency spectrum bound all the spectra of all reasonable physical waveforms. There can, of course, be other important considerations, particularly when one deals with some kinds of nonlinearities.

Another studied portion of the HEMP waveform is that for very late times associated with the plasma expansion (heave) in the presence of the Earth's magnetic field. This is termed the magnetohydrodynamic EMP (MHD-EMP), covering times from a fraction of a second to a few minutes. The peak horizontal electric field can be 10 s of millivolt per meter (or 10 s of volt per kilometer) [131]. It has some similarity to geomagnetic storms and is of concern to systems with very long conductors, such as commercial power and communications.

B. Surface-Burst EMP

Within a few km of a surface burst there are strong fields near the ground surface, these being relevant to buried, hardened facilities. This environment is discussed in some detail in [85] and [168]. The source region (where conduction current dominates displacement current in the air) has Compton current density of order 1 A/m^2 and air conductivity of order 10^{-4} S/m at the edge of the source region (about 1 MGy/s or 10^8 rad/s), scaling with the γ-ray intensity as one goes inward toward the detonation point. Note that significant radiation still extends beyond this distance and often needs to be considered in source region interaction problems. Electric fields peak at a little over 10^5 V/m (saturation given by J_c/σ), but the associated conduction current density (very important for interaction) scales with J_c and hence the γ-ray intensity. The magnetic fields are generated within a diffusion depth of the ground surface and scale roughly as (γ-ray intensity)$^{1/2}$. The peak magnetic flux density in the source region is of the order of 6 mT and has a pulsewidth of the order of 100 μs, while the electric field decays much faster. Both fields rise in a few 10 s of nanoseconds. Long buried cables under this source region can have currents of order 100 kA rising in 100 μs with 1 ms-width.

C. Direct-Strike Lightning

While lightning has been around for a long time, it is only recently that we have begun to obtain some detailed theoretical and experimental information concerning the lightning discharge, particularly for the rapidly time-varying parts. Part of the reason for this concerns modern developments concerning electromagnetic sensors (Section III) and fast digital recording instruments. Much of the modern

lightning-arc physics is included in a recent book [15]. There are standard references which include the extensive distant measurements and atmospheric processes (charging, etc.) [12]–[14], [16], [184]. Here we concentrate on the close-in (direct-strike) environment.

Consider the often-used waveform for the lightning current in Fig. 3. This is, of course, a simplification of the real environment which has a somewhat more jagged time history. Here we have used a QEXP waveform as in (2.4) with parameters chosen to give a peak dI/dt of 2×10^{11} A/s (reasonable worst case) and peak currents of 100 kA (reasonable worst case) and 10 kA. The exponential decay rate is taken as 50 μs. In a given strike something like this environment may repeat (subsequent return strokes) up to about 20 times. Of course, one can increase the environment in testing for an engineering safety margin, but this applies to all HPE environments (e.g., HEMP).

This lightning environment is not as well understood as the HEMP environment as is evidenced by the lack of electric-field (or surface-charge-density) specifications on systems struck by lightning. As one would expect electric fields of the order of air breakdown [16(Baum *et al.*, pp. 123–137)], [161] (a few megavolts per meter) on struck aircraft, etc., such should be included. Furthermore this is accompanied by the corona and lightning arc associated with air breakdown. The corona affects the electric response of apertures and antennas. The arc is part of the system electromagnetic geometry, changing the exterior resonances [15(Yang and Lee, pp. 75–86), (Gardner *et al.*, pp. 491–533)]. Experimental results from direct strikes on the NASA F-106 show that in a peak sense E/H ratios can vary considerably (order of magnitude) with the ratio typically large compared to Z_0 [15(Gardner *et al.*, pp. 491–533)], [116]. The physical processes in lightning interaction are qualitatively more like surface-burst EMP than HEMP, but quantitatively quite different.

Concerning the lightning-arc physics there has been some significant progress in modeling. Numerical models including the hydrodynamics and optical radiation transport (as well as air conductivity) have been published [15(Paxton *et al.*, pp. 47–61), (Baker, pp. 63–74)]. There are also analytic results based on a simplified corona model [15(Baum, pp. 3–16), (Baum and Baker, pp. 17–40), (Baum, pp. 101–114)]. This is a part of a transmission-line model in which the inductance per unit length is based on an arc radius (carrying most of the current) in the mm range. The capacitance per unit length is based on a corona radius of some meters (corona surrounding the arc) given by a breakdown electric field (a few megavolts per meter) and the charge per unit length. Neglecting losses in arc and corona analytic equations (nonlinear) are developed with analytic solutions. There is a shock solution for the return-stroke speed as

$$\frac{v}{c} \simeq \left[\ln\left(\frac{\Psi_\infty}{\Psi_o}\right)\right]^{-1/2}$$

Ψ_o = arc radius

Ψ_∞ = effective outer radius in transmission-line model. (2.7)

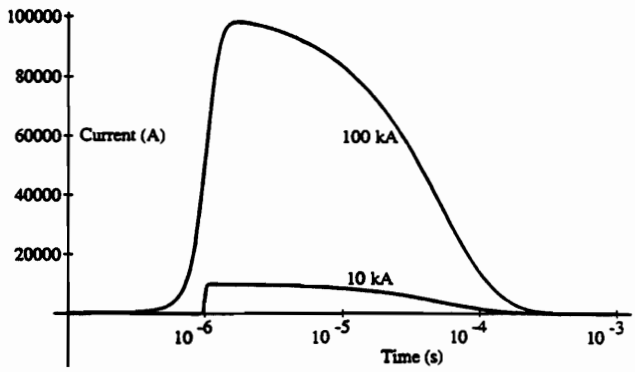

Fig. 3. Direct-strike lightning current waveforms.

Typical numbers give v as about $c/3$ as observed, with currents 100 kA. (Note that this corona model can also be applied to the response of wires in corona [93].)

While the above is appropriate for a circular cylindrical initial corona, this is not an appropriate geometry for the return-stroke initiation region near the ground. Here the corona has not had time to grow to several meters in radius. A more appropriate geometry is a circular bicone (downward leader meeting upward leader from ground) with the conical apex as the initiation point. In this case analytic results [15(Baum, pp. 101–114)] give an initial return-stroke speed of nearly c. Recent simultaneous measurements of both current and nearby fields are consistent with this result [15(Baker *et al.*, pp. 365–374)], [152], [171]. One should note, however, that other processes can also contribute to the variation in current versus fields produced in the return stroke [15(Baum, pp. 101–114)], [148]. So it is risky to infer return-stroke currents, at least in the early phase, from distant field measurements (except perhaps in an order-of-magnitude sense).

Looking at some of these HPE environments some have considered the question of what testing to one tells about response to another. Specifically there are several papers addressing the comparison of aircraft responses to HEMP and direct-strike lightning [15(Gardner *et al.*, pp. 491–533)], [137], [142], [144]. Looking at the frequency spectrum of the surface fields from environmental models and actual tests of aircraft (simulated HEMP, but natural lightning) one finds that below about 1-MHz lightning dominates, but above roughly 10-MHz HEMP dominates. In the external-resonance region in this gap the question is not well resolved yet due to the shift of these resonances by the lightning arc. It is interesting to note that typical internal transient responses have been larger for HEMP than for lightning, but one should not expect this to always be the case. Note also that lightning also can give mechanical damage (pitting of metal, destruction of dielectrics (potentially catastrophic)) associated with the slower parts of the pulse. So the general conclusion is that one needs both kinds of tests. Hopefully, some kind of specifications and standards to design and test for both environments can be evolved. Note, however, that (as discussed in Section VI) survival

may be defined differently for the two environments (e.g., mission completion for HEMP versus landing safely for lightning).

D. HPM

Unlike the previous environments, HPM is in a state of development which makes it very difficult to specify some particular environment or family of environments. It depends on the source, radiating antenna, frequency, range, etc. One could specify limits based on air breakdown at the system but these would be way too large in general. As discussed in Section V-B, the environment would consist of a basically single-frequency waveform tuned to some system resonance for maximum interaction, this giving an order of magnitude more signal inside the system at positions of interest. There are also trade-offs involving antenna directivity and source power as a function of frequency, as well as breakdown limitations at the transmitting antenna. The present is too soon to be definitive.

III. Environment and Response Measurements

An important part of this technology concerns the measurements of large, fast-rising electromagnetic fields and related parameters such as currents and voltages. This can range from plane waves in free space to ionized regions near lightning arcs or nuclear source regions. Furthermore, one often measures fields in the presence of complex structures (system under test), such as on the system exterior (surface current and charge densities) or inside the system (currents and voltages on wires and various places in electronic equipment).

Much has been written about these sensors for which the reader can consult several reviews. [1(Baum *et al.*, pp. 22–35)], [16(Baum *et al.*, pp. 123–137)], [8], [9], [45], [139], [155]. Here we will briefly review some important points in sensor design and then consider some new developments.

In sensor design it is important to note that the problem is design (or synthesis), not analysis. One can analyze various geometrical structures of varying degrees of complexity and consider some current or voltage somewhere on this structure as a potential antenna port. But then, what are the pattern, sensitivity, and frequency (or transient) response characteristics of this antenna? Furthermore, are these appropriate (or better, optimum) for our measurements. The detailed definition of a sensor for our purposes is discussed in [1(Baum *et al.*, pp. 22–35)], [8(Baum, pp. 73–144)], [9(Pressley and Sower, pp. 175–210)]. Briefly summarizing it is a passive analog device converting the EM quantity of interest to a voltage or current of a port, the sensitivity being accurately calculable in the frequency band of interest (calibratable by a ruler), and the bandwidth being optimized within the above constraints.

For general electromagnetic field measurements (the character of the fields unspecified except for satisfying the Maxwell equations without sources) the basic types of sensors are based on electric and magnetic dipole moments, being the leading terms in a multipole expansion (oscillating monopoles not being allowed in electromagnetics with currents confined to a bounded volume [179]).

An electric-dipole sensor has vector equivalent areas and lengths related via a capacitance (and permittivity) as

$$\vec{A}_{e_{eq}} = \frac{C}{\epsilon}\vec{\ell}_{e_{eq}}. \tag{3.1}$$

For short-circuit measurements this measures the displacement current density via

$$I = \vec{A}_{e_{eq}} \cdot \frac{\partial \vec{D}}{\partial t}. \tag{3.2}$$

Note that if the medium is conducting (conductivity σ) then there is a conduction current density $\sigma\vec{E}$ in this equation as well and there is a conductance G in parallel with capacitance related to the permitivity ϵ via

$$\frac{G}{\sigma} = \frac{C}{\epsilon} \tag{3.3}$$

provided the sensor does not include insulators which interfere with conduction current flow to the antenna conductors (assumed "perfectly" conducting), i.e., provided σ is distributed like ϵ [59]. Open-circuit measurements are for the electric field via

$$V = \vec{\ell}_{e_{eq}} \cdot \vec{E}. \tag{3.4}$$

Depending on the type of sensor desired, it is area or length which is to be accurately known and designed to have a convenient numerical value (magnitude).

A magnetic-dipole sensor has vector equivalent areas and lengths related by an inductance (and permeability) as

$$\vec{A}_{h_{eq}} = \frac{L}{\mu}\vec{\ell}_{h_{eq}}. \tag{3.5}$$

For open-circuit measurements this measures the magnetic flux density via

$$V = \vec{A}_{h_{eq}} \cdot \frac{\partial}{\partial t}\vec{B} \tag{3.6}$$

while the short-circuit version is for the magnetic field as

$$I = \vec{\ell}_{h_{eq}} \cdot \vec{H}. \tag{3.7}$$

There are some figures of merit appropriate to these dipole sensors related to the trade-off between size, bandwidth, and sensitivity. For low-frequency sensors (electrically small for all frequencies of interest) there is an equivalent volume related to the energy extracted from the incident field and delivered to the load as

$$V_{e_{eq}} = \vec{A}_{e_{eq}} \cdot \vec{\ell}_{e_{eq}}, \quad V_{h_{eq}} = \vec{A}_{h_{eq}} \cdot \vec{\ell}_{h_{eq}} \tag{3.8}$$

where this is of the order of the geometrical volume of the sensor. For the fast time-derivative dipole sensors limited

by transit times across the sensor (or wavelength compared to size) there is a figure of merit

$$\Lambda_e = \left(\frac{Z_c}{Z_0}\right)^{1/2} \left|\vec{A}_{e_{eq}}\right| \ell_c^{-2}, \quad \Lambda_h = \left(\frac{Z_0}{Z_c}\right)^{1/2} \left|\vec{A}_{h_{eq}}\right| \ell_c^{-2}$$

$Z_c \equiv$ resistive load driven by sensor (transmission-line characteristic impedance)

$\ell_c \equiv$ length characteristic of temporal resolution or bandwidth

$$= ct_c = \frac{c}{\omega_c}. \tag{3.9}$$

Note that this figure of merit takes the form sensitivity (bandwidth)^2 and is not a function of the sensor size (scale invariant) but is a function of the shape and impedance loading. Since the sensors of interest incorporate various symmetries for optimum dipolar response, there is normally a symmetry plane that can be used to divide the sensor in half for mounting on metallic planes and thereby measuring surface fields (or surface current and charge densities). In such cases there are factors of two that appear in the capacitance and inductance, area of length and the load impedance. So it is convenient to consider a particular sensor design efficiency in terms of its free-space (instead of ground-plane) version. A different case has the sensor constructed as a special aperture in the ground plane [54].

This characteristic length ℓ_c related to bandwidth needs some close consideration. For this purpose we need a more precise definition of what is an ideal dipole sensor for point field measurements. This is done in [48] based on a multipole expansion of the sensor response. Briefly summarizing, let the incident plane wave be specified by the direction of incidence $\vec{1}_1$ and a polarization $\vec{1}_{\substack{e\\h}}$ applying to the electric or magnetic field of interest. Letting the area vector be parallel to the z axis, let the polarization be in the plane of $\vec{1}_1$ and $\vec{1}_z$. The sensor should be in general insensitive to the orthogonal polarization, even at high frequencies, particularly with sufficient symmetry (with respect to the xy plane and z axis) incorporated in the sensor design. Specifying the direction of incidence by spherical angles θ_1, ϕ_1 we have the output voltage of the sensor $\tilde{V}(\theta_1, \phi_1; s)$ into the constant resistive load Z_c. Then appropriately weighting over the spherical angles gives

$$\tilde{g}(s) = \frac{3}{4\pi} \int_0^{2\pi} \int_0^{\pi} \tilde{V}(\theta', \phi'; s) \sin^2(\theta')\, d\phi'\, d\theta'$$

$$\tilde{g}(s)\sin(\theta_1) = \text{dipole part of response.} \tag{3.10}$$

So a first way to look at sensor bandwidth concerns this frequency function $\tilde{g}(s)$.

At low frequencies this function goes to the ideal sensor response as

$$\tilde{g}_e(s) \to \tilde{g}_{e_0}(s) = Z_c s\epsilon \tilde{E}_{\text{ref}}(s) \left|\vec{A}_{e_{eq}}\right| \quad \text{as} \quad s \to 0$$

$$\tilde{g}_h(s) \to \tilde{g}_{h_0}(s) = s\mu \tilde{H}_{\text{ref}}(s) \left|\vec{A}_{h_{eq}}\right| \quad \text{as} \quad s \to 0 \tag{3.11}$$

where the reference fields refer to the polarization direction $\vec{1}_{\substack{e\\h}}$. Normalizing the actual dipole response to the ideal form gives

$$\tilde{G}_{\substack{e\\h}}(s) = \frac{\tilde{g}_{\substack{e\\h}}(s)}{\tilde{g}_{\substack{e_0\\h_0}}(s)} \to 1 \quad \text{as} \quad s \to 0 \tag{3.12}$$

the deviation of $\tilde{G}$ from 1 being a way to define the sensor bandwidth, a traditional choice for $|G(j\omega)|$ being $1/\sqrt{2}$.

Deviation of the dipole part is not the only error. At high frequencies the angular response deviates from the dipole response. To treat these angular errors one can form an error function via

$$\text{error} = \frac{\left\|\tilde{V}(\theta_1, \phi_1; j\omega) - \tilde{g}_{\substack{e\\h}}(j\omega)\sin(\theta_1)\right\|}{\left\|\tilde{g}_{\substack{e\\h}}(j\omega)\right\|} \tag{3.13}$$

where the norm is taken over the unit sphere. Many norms can be chosen, common ones being the ∞-norm (peak) or 2-norm. Assigning some allowable angular error in (3.13) gives an ω which can be compared to that in (3.12) as an alternate definition of bandwidth. Of course, both can be used and the smaller frequency used to define the bandwidth.

These parameters have been measured for some common sensor designs [46]. The asymptotic conical dipole (ACD) is a D-dot sensor based on an equivalent-charge method for specifying the sensor shape which allows accurate calculation of area, height and capacitance. As discussed in [8(Baum, pp. 73–144)], a uniform line charge of finite length is assumed on the $+z$ axis (with image on the $-z$ axis). The quasi-static potential surface which defines the sensor shape is like two tear drops which are a body of revolution asymptotically approaching a symmetrical circular bicone (of characteristic impedance 100 Ω) near the coordinate origin which gives a high-frequency match to the two 50-Ω coaxial output cables. The figure of merit Λ_e is about 2.7 using a $1/\sqrt{2}$ value for $|\tilde{G}_e|$. The bandwidth in this sense corresponds to an overall sensor length of about a quarter wavelength, and the length is a little less than the rise time times c. For the angular error in (3.13) defined in a peak sense (∞-norm) with a value of 0.3 the corresponding frequency is about 2.5 times that defined in the $\tilde{G}_e$ sense so that the angular error is not significant. Figure 4 shows an example, the ACD-6 with an equivalent area of 0.1 m^2, this being a ground-plane version with 50-Ω coaxial output. This is a more recent version with some improvement in the shape based on the addition of point charges at the extreme of the line charge on the z axis [58]. This makes the teardrop somewhat fatter and avoids a slight peaking up of the sensor response $\tilde{G}_e$ before it drops off at the upper bandwidth.

The multigap loop (MGL) is a B-dot sensor with an accurately known equivalent area. As discussed in [8(Baum, pp. 73–144)] the basic structure is a finite length (about one diameter) circular cylinder to reduce inductance (as compared to a wire or toroidal loop). There are four loop gaps around the cylinder to remove unwanted higher order terms in the response (such as the "electric-field" response),

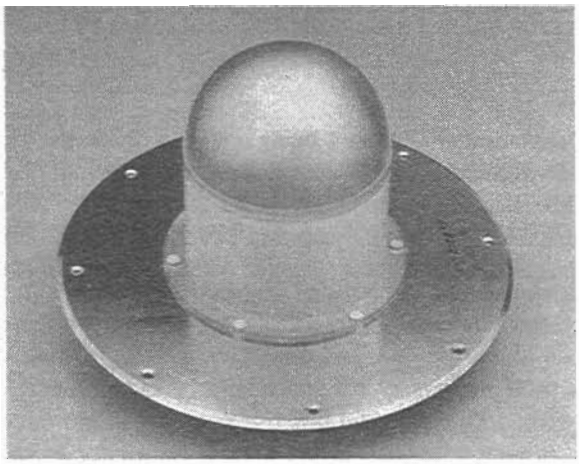

Fig. 4. ACD-6B(A) D-dot sensor.

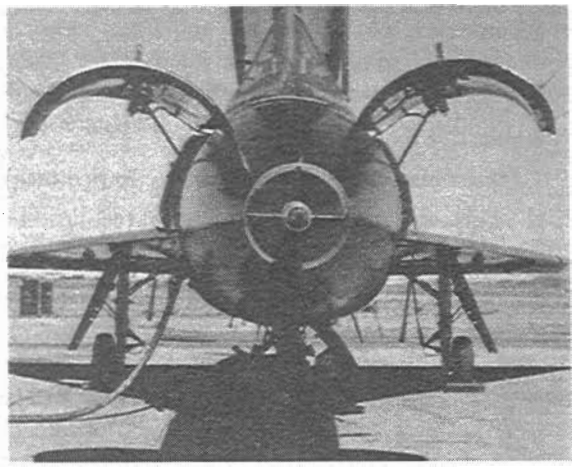

Fig. 5. MGL-2E(AM) B-dot sensor mounted on pitot-static nose boom of NASA F-106B research aircraft.

effectively by an increase in symmetry. Each loop gap has two parallel 200-Ω signal-pickoff positions from a local gap geometry as a 200-Ω conical transmission line. There are divider plates between the loop gaps dividing the loop into four quadrants, the signals being combined via transmission lines in a series/parallel combination so that the equivalent area is half the geometrical area. The figure of merit Λ_h is about two using a $1/\sqrt{2}$ value for $|\tilde{G}_h|$. Again the bandwidth in this sense corresponds to a sensor diameter of about a quarter wavelength, and the diameter is a little less then the rise time times c. The angular error in (3.13) defined in a peak sense as 0.3 again gives a corresponding frequency of about 2.5 times that defined in the $\tilde{G}_h$ sense and is insignificant. Figure 5 shows an example, the MGL-2 with an equivalent area of 0.01 m^2. The particular model shown is mounted on the aircraft symmetry plane with location and orientation so as to reduce the error in incident-field measurements (due to aircraft scattering) to a few percent [49], [125]. In the particular application shown one can see the sensor interior. Usually there is a plastic cover to keep people, water, etc., out, this being removed to allow the in-flight airstream to flow through the sensor. The output cables (two 50-Ω coaxes) are contained inside the pitot boom which had to be allowed for in the equivalent area for accuracy in this application. Note also the use of printed circuit board (typical) which is etched to leave the metal for the detailed outer loop geometry including some of the summing transmission lines (strip lines).

There are of course various other designs of dipole sensors for various frequency-response/transient characteristics. Of particular interest is the balanced transmission-line wave (BTW) sensor which balances electric- and magnetic-dipole characteristics to give a directional coupler for plane waves [36], [61], [69]. One can use reciprocity and consider such a device as a $\vec{p} \times \vec{m}$ antenna in which the dipole moments are balanced with

$$\vec{p} \cdot \vec{m} = 0, \quad |\vec{p}| = \frac{1}{c} |\vec{m}|$$
$$\vec{p} \equiv \text{electric dipole moment}$$
$$\vec{m} \equiv \text{magnetic dipole moment.} \qquad (3.14)$$

Such an antenna radiates in the $\vec{p} \times \vec{m}$ direction (maximum) with a null in the opposite direction. The BTW design involves a small TEM transmission line terminated in its characteristic impedance. When the length is electrically small then (3.14) applies and the $\vec{p} \times \vec{m}$ direction is from the source in the opposite direction to the transmission line, and so as a sensor it is sensitive to waves traveling parallel to the direction to the termination, the source end feeding the sensor output with the same impedance as the transmission line. There are various other geometries which can in principle be utilized to obtain this property, and perhaps some optimization of the design will occur in the future. It has important uses in various applications where one wishes to discriminate between incident and reflected waves, such as in hybrid EMP simulators (Section IV) for incident from ground-reflected fields, and in guided-wave EMP simulators to aide in optimizing the design of the simulator termination.

There are various other types of antennas for measuring fields, depending on the specific measurement conditions. The dipole type of sensor can be adapted to measurements in conducting media and even to cases of nonlinear, time-changing media with sources as in the case of nuclear source regions and lightning [8(Baum, pp. 73–144)], [59]. One can also use non-dipole designs in special cases where certain characteristics of the incident field (e.g., plane wave, direction of incidence, and polarization) are accurately known *a priori* [146]. Another field-related quantity is the surface curl of the surface current density ("dual" to the surface divergence giving surface charge density). This type of measurement leads to a magnetic-quadrupole sensor [50].

Current sensors are another area which has received a lot of development [155]. For the fast l-dot sensors this basically involves the various distribution and cable-topology techniques used in the B-dot sensors, except that the (rectangular) cylindrical loop is extended in axial length and bent around to have the ends join to give a donut-like shape [8(Baum, pp. 73–144)]. The fastest of these are limited to bandwidth only by transit times on the sensor

structure. Figure 6 shows an example set of sensors as installed on South Baldy Peak, Socorro, NM, to measure lightning currents [130]. This is an array of three sensors built into a cylindrical post on which the current is flowing. From the top there is a resistive shunt (limited in rise time by diffusion through the metallic foil), second there is an I-dot sensor (sub ns), and third there is a more conventional current transformer with a magnetic core. Note that the sensors are configured so as to measure the current on the outside of the post, and the lower two sensors provide shielding for the interior of the post to allow the topological configuration of the sensor-output cables down the inside of the post to the interior of the shield room below the ground plane on the mountain top [8(Baum, pp. 73–144)].

Voltage sensors (high impedance) are often problematical, but the divider strings (resistive and/or capacitive) can be made to minimally distort the fields in the vicinity of the measurement [8(Baum, pp. 73–144)]. This can be an important consideration, especially in fast, multimegavolt pulse-power equipment.

There is various auxiliary equipment sometimes used with sensors. Special transformers (baluns) are used to change impedances and convert between single ended and differential. These are for convenience in signal transmission (e.g., input to modulators for data transmission) or for generating particular kinds of signals on special antennas (e.g., low level EMP simulators). The cable-topology techniques used in sensor design are extended into transformer design [104], [106], [107]. The two or more windings in a usual transformer are replaced by shielded cables with the shields bonded together to appear as a single winding to the core and thereby remove leakage flux between the windings. Breaks in the cable shields are used to transmit signals from one cable to another with gap structures (single ended, differential (Moebius)) similar to those used in loop design. Thereby extremely large bandwidths and accurate transfer functions are obtained.

The recording aspect is common with various other technologies involving oscilloscopes and transient digitizers. Data transmission, however, can have some special problems. In some cases one can use well-shielded coaxial cables to accurately transmit the fast signals. In such cases this is the desirable approach due to improved bandwidth, linearity, and signal-to-noise ratio. Note that the derivative sensors in the large environments can put out typically hundreds of volts. However, these cases are restricted to ones in which the experimental topology and/or symmetry in the measurement geometry allow the signal cables not to interfere with the measurement by electromagnetic scattering [8(Baum, pp. 73–144)]. In the topology aspect one is allowed to route cables along the system conductors (with cable shield bonded to these conductors frequently along the route), jumping no gaps in such conductors (e.g., along bulk heads, hulls, trays, metal beams, etc., in ships, aircraft, buildings, etc.). In some cases (e.g., simulator ground planes) one has an effective shielding surface which one can use to "hide" signal cables away from the HPE environment.

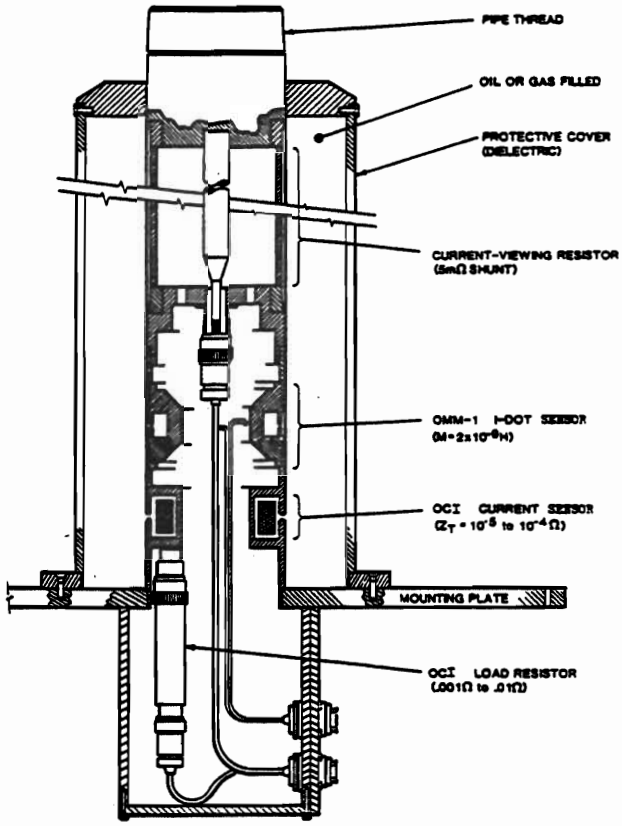

Fig. 6. Cutaway view of the EG&G lightning current measuring sensor array on Kiva 2.

For many cases, however, one needs electrical isolation between the sensor and recorder. In such cases the commonly used technique in current use is fiber-optic data links [8(Chandler, pp. 419–435)], [133], [154], [156]. There is also the general problem of correction of data to allow for various imperfections in transfer functions as well as noise between sensor and recorder. This involves numerical Fourier transforms and deconvolution techniques [8(Nahman, pp. 351–417)], [167], [170]. This is by no means a simple problem in practice.

IV. Environmental Production and Simulation

One of the most important developments from EMP technology concerns the generation of large, fast-rising EM transients and the radiation and propagation of these in a variety of geometries. This has been associated with the design of EMP simulators concerning which one can consult reviews with many references [1(Baum, pp. 35–53)(Smith and Aslin, pp. 53–59)], [2], [158].

The most prevalent kinds of EMP simulators are those for the high-altitude EMP [1(Baum, pp. 35–53)], [145], [160], there being three common general types, depending on the particular application. The first of these is the guided-wave or transmission-line type [41], [157]. These are particularly appropriate for testing missiles and aircraft in flight, since such simulators are designed to ideally produce a single TEM wave. This approximates a single uniform plane wave, at least in the vicinity where the system is to be tested. Conveniently, such structures present an approximately

constant resistive impedance to the pulse power source. For high-field applications where efficiency and avoiding breakdown are important the conductors are wide plates (meshes typically) with roll-ups on portions of the edges [57]. There are conical launch sections leading from the pulsers, followed by cylindrical (parallel-plate) sections and additional conics leading to terminators. These are out in the open environment instead of in shield enclosures which would greatly increase the cost and significantly complicate the electromagnetic environment (e.g., cavity resonances). Various large ones have been built, with the largest, the ATLAS I as in Fig. 7 being 400-m long, 75-m high, and 105-m wide, in a differential configuration for testing large aircraft. Also notable is the test stand, a trestle reputed to be the largest wooden structure in the world.

For the smaller to medium size of this type of simulator a popular modern option consists of an extended version of the input conic to propagate the conical TEM mode over the system under test, going directly to a large distributed terminator [1(Baum, pp. 35–53)], [128], [129]. This shortens the overall length somewhat, saving real estate. This type exists or is being constructed in various European countries including Sweden, Germany, France, Switzerland, and Italy. From a technical performance point of view there is a tradeoff between the problem, on the one hand, of matching the TEM mode from one conic to a cylindrical section and then to an output conic without significant higher order modes (TE and TM) present [38], [126], [127], [132], [134] and, on the other hand, of designing the large distributed terminator to not send significant reflections back to the system under test [129]. From an analytical point of view there is some considerable understanding of these modes. For the cylindrical (parallel-plate) section the TEM mode is extensively tabulated [27] and the higher order modes (and continuous spectrum) have received some attention [24], [25], [30], [31], [39], [40], [42], [43]. For the conical (flat plate) section some results have been obtained for the TEM mode [28], [32], [33]. While volts divided by spacing gives an approximate value for the electric field between the plates, the above references can be consulted for more accurate estimates.

For low-level (e.g., CW) applications one need not have a continuous plate (typically mesh) which is required for supporting a high electric field (without breakdown at the plate) and achieving some efficiency in terms of electric field per volt (noting the megavolts required). Then one can conveniently use two wires on a diverging conical configuration above the ground surface in both common and differential modes (the GEMELLUS concept) with resistive loading in the termination two-wire conic to achieve a smooth (and flat) quasi-TEM performance [135], [136], [141].

The second common type of simulator for the high altitude EMP is the hybrid, an example is given in Fig. 8. This type of simulator is intended to produce an approximate incident plane wave at the system under test, and include the reflected plane wave from the Earth surface. As such it is suitable for testing such systems as fixed sites (not too large), parked aircraft, etc. The design principles are summarized in [47] with appropriate references.

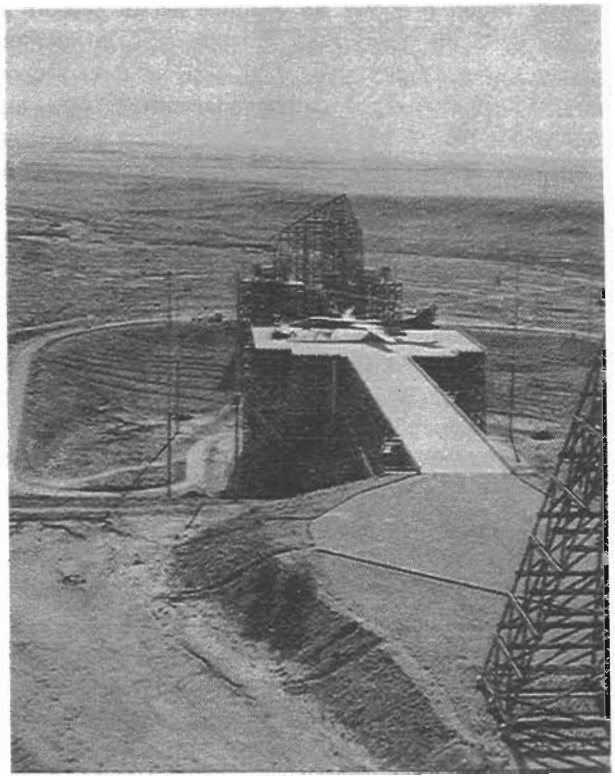

Fig. 7. ATLAS I (B-1B under test).

Fig. 8. ATHAMAS I (French Aircraft under test).

The concept of such a hybrid simulator involves three aspects. At early times (high frequencies) the wave is dominated by features of the antenna near the pulser, this region normally being in the form of a circular bicone, the pulse impedance Z_a (valid only for early times) being typically 120–150 Ω. Assuming a sufficiently fast rise time of the pulse, the peak electric field incident at some distance a' from the bicone apex and normal to the bicone axis is

$$E_0 = \frac{Z_0}{2\pi Z_a}\,\frac{V_0}{a'} \simeq \frac{60\ \Omega}{Z_a}\,\frac{V_0}{a'}$$
$$V_0 \equiv \text{peak pulser voltage.} \qquad (4.1)$$

For low frequencies (or late times if the pulsewidth is much greater than transit times across the structure) the fields in the immediate vicinity of the simulator structure are quasi-static in nature. As the system under test is intended to be in this immediate vicinity (even in some cases directly under the arch) this quasi-static performance for the low frequencies is intentional. First (for purpose of analysis) consider a full loop in free space. Based on a circular loop (toroid) of major radius a and minor radius b the loop is loaded with a resistance per unit length R' given by

$$R' = \frac{Z_0}{2\pi a}\left\{\ln\left(\frac{8a}{b}\right) - 2\right\} \tag{4.2}$$

so that

$$\frac{E}{H} \simeq Z_0 \quad \text{(free space wave impedance)} \tag{4.3}$$

at the center of the toroid at low frequencies. (One could use such a free-space hybrid to give a single plane wave (approximately) but at a significant loss of efficiency in terms of electric field per volt.) Of course, including the Earth surface, there is the desired reflection which at high frequencies is governed by plane-wave reflection formulas, and at low frequencies is approximately described by image theory (image antenna and pulser). The low-frequency content of the magnetic filed at the center of the loop (including image) is described by

$$\tilde{H}(0) \simeq \frac{\tilde{I}(0)}{2a} = \frac{Q_g}{2a} = \frac{V_0 C_g}{2a} \tag{4.4}$$

where C_g is the generator capacitance and Q_g the charge. Note that a represents an average radius in the case of the actually used elliptical shape. Furthermore b represents an effective minor radius, allowing for the practical use of a wire cage (resistively loaded) for the antenna.

For intermediate frequencies (wavelengths of the order of a) one needs a smooth transition from the high-frequency to low-frequency performance. This is achieved by the sparse (thin) nature of the antenna, so that waves reflected from the Earth mostly propagate out of the region (at these intermediate frequencies), instead of rattling around inside a more enclosing structure. This is further aided by the resistive loading of the antenna providing additional damping.

There is also the design problem of transitioning from the bicone near the pulser to the wire cage. One minimizes any sharp discontinuities by going from the bicone to a circular cylinder, and then through triangular tapers to the wires.

More recently seminanalytic models have been developed with transmission-line approximations for the currents on the antenna [65], [175]. While these have some limitations they can tie the intermediate- and low-frequency behaviors. These apply best for antennas with b/a very small, which are not the case for high level environments, but which are the case for low level environments [81] (e.g., CW for hardness maintenance use). Of course one can use more general numerical techniques for analyzing the response of such an antenna [74].

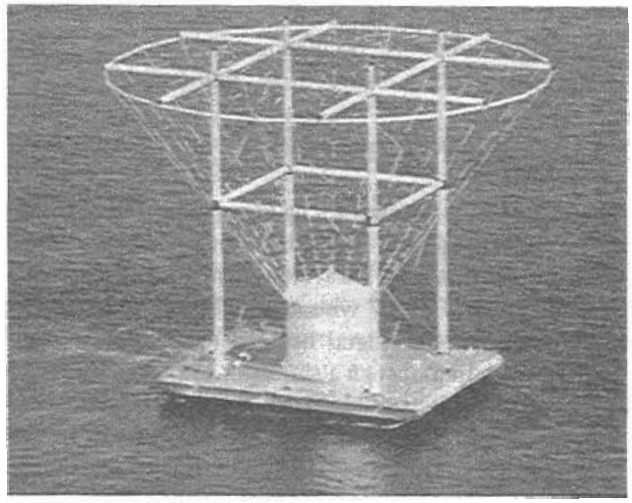

Fig. 9. EMPRESS II.

The third type of HEMP simulator is the equivalent electric dipole, an example being given in Fig. 9. This has an optimum use in a more specialized role. For various reasons the simulator must be kept some distance away from the system under test. For example, if the system under test (e.g., a large ship) is larger than the simulator (the ATHAMAS II and EMPRESS II being 40-m tall) then one cannot be very close and still have an approximate plane-wave environment. In another application one might have an actual flying aircraft under test. Of course the distances reduce the field levels indicating a performance trade-off. The design principles are summarized with references in [1(Baum, pp. 35–53)], [47].

The antenna takes the form of a resistively loaded circular cone centered on a vertical z axis. If the angle of the cone is θ_0 from the z axis the high-frequency (early-time) impedance is

$$Z_\infty = \frac{Z_0}{2\pi}\ln\left[\cot\left(\frac{\theta_0}{2}\right)\right] \tag{4.5}$$

with values of 60–75 Ω being typical. Because of the ground plane (near the antenna) this is half that of Z_a in (4.1). This gives a peak field at some distance Ψ (near the Earth surface) for sufficiently fast pulser rise of

$$E_0 = \frac{Z_0}{2\pi Z_\infty}\frac{V_0}{\Psi} \simeq \frac{60\ \Omega}{Z_\infty}\frac{V_0}{\Psi}. \tag{4.6}$$

Now the fundamental problem with such a radiating type of simulator is its limited low-frequency performance in the far field. (Antennas do not radiate dc!) Consequently it is important to do as best one can for such frequencies. The low frequencies are dominated by the late-time equivalent electric-dipole moment $\vec{p}(\infty)$ which is the equivalent height times the late-time charge, this in turn being given by the pulser voltage and a capacitive division between pulser and antenna capacitance. So the low-frequency content goes roughly like height squared times voltage, with some help from the antenna fatness. The addition of a top cap on the cone also helps.

To smooth out the waveform for intermediate times and frequencies (minimize oscillations) the antenna is resistively loaded with a resistance per unit length

$$R'(z') = \frac{Z_\infty}{h'}\left[1 - \frac{z'}{h'}\right]^{-1} \qquad (4.7)$$

where z' is the slant distance up the cone and h' is the slant height. Near the top ($z' = h'$) this is smoothed over onto the top cap. This produces a waveform (far field) with one zero crossing at $ct/h' \simeq 0.7$ with about 20% or so undershoot, the complete time integral being zero as required. More detailed modeling of such a simulator can be accomplished, including the effects of the lossy Earth [72], [73].

For simulating close-in EMP (source region) near the Earth surface less work has been done. As discussed in [1(Baum, pp. 35–53)] the SIEGE simulator design employs a buried transmission line with low frequency portions of the pulse propagating downward in an approximate TEM mode in the lossy Earth. The higher frequency portions are handled by a surface transmission line with a conducting plate (grid) above and parallel to the Earth surface. The DISCUS concept involves a set of distributed sources to launch the wave into the Earth surface and some considerable progress has been made [44], [51], [52], [55], [71]. With individual wave launchers of 1 m × 2 m (looking like butterflies), transmission-line and high-frequency Brewster angle concepts allowed achieving rise times of the fields in the upper regions of the soil of a few nanoseconds.

Related to EMP simulators is the design of antennas and associated pulse power and switching for transient radars. One class of such is the kind one might use in the context of the singularity expansion method (SEM) for target discrimination using natural frequencies (aspect independent) and residues (target polarization) [2], [4(Baum, pp. 129–179)], [99], [100], [181]. In this case the desired radiated waveform is dependent on the class of targets of interest, since the important frequencies in the pulse are those in the range of the target complex natural frequencies. For aircraft this is the HF band, requiring large antennas, such as the equivalent-electric-dipole type (discussed above) with various modifications to optimize the waveforms (e.g., damped sinusoids). This is discussed in a recent article [153].

Another type of transient radar of interest is sometimes referred to as an impulse radar in that a very narrow pulse (perhaps subnanosecond) is desired, such as for range resolution over the target. From an antenna point of view one can think of various types of directive broadband antennas (e.g., [174]). However, one should also incorporate various techniques used in EMP simulators to optimize the waveshape (e.g., minimize dispersion and control appropriate reflections) and increase the pulse power it can handle. As illustrated in Fig. 10 one can combine the concept of a focusing reflector with the typical type of TEM feed used in a guided-wave EMP simulator [70], [76]–[79]. Launching a fast-rising (step-like) TEM wave on the conical wave launcher, the wave is reflected and approximately

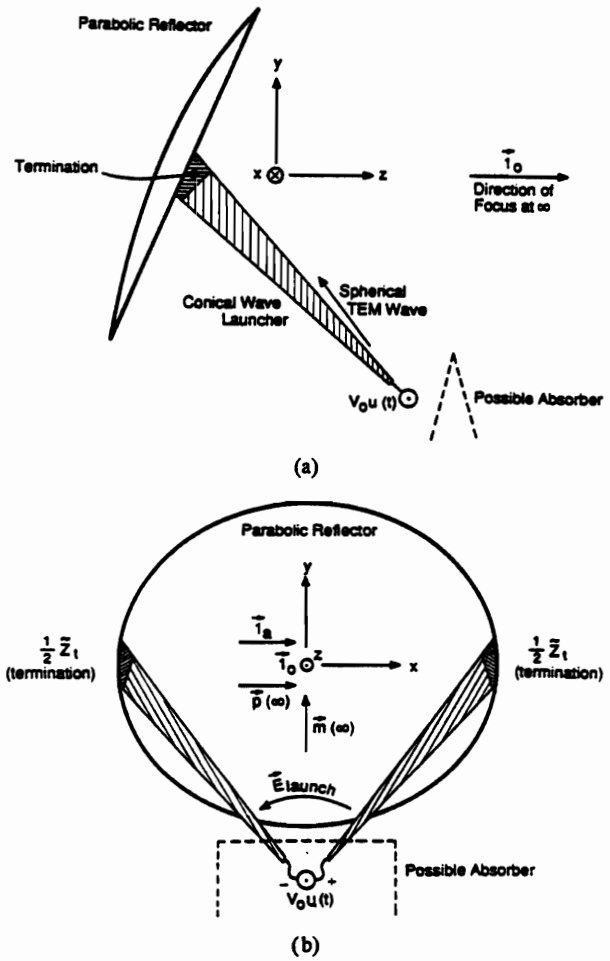

Fig. 10. Conical TEM wave launcher feeding reflector. (a) Side view and (b) front view.

time differentiated for large distances in the focal direction. Note the termination (resistive) of the conic at the reflector to minimize multiple reflections. Of course the waveform is complicated by various factors such as the direct signal from the conic and the fact that the complete time integral must be zero. The illustration in Fig. 10 includes only the basics. Various features can be added such as conductors (including signal feeds) on the y, z plane, baluns [111], and dual polarization from two "orthogonal" conical wave launchers [76].

In going to faster and faster rising pulses of high amplitude one runs into a problem (for both EMP simulators and impulse-radar antennas). Extrapolating the desired TEM-mode fields back toward the conical apex, the electric-field magnitude at some radial distance exceeds the breakdown strength of air. Allowing for non-ideal operating conditions, for EMP simulators with pulsewidths of order 100 ns this is about 1 MV/m. With a dielectric diaphragm (thin so as to not distort rise time) one can introduce a higher dielectric strength gas such as SF_6 or freon at local atmospheric pressure to roughly triple the breakdown strength. The conical transmission line can be continued until this limit is reached. Then one can increase the gas pressure, but this requires a dielectric pressure vessel with thick walls. This can be done in more than one stage if desired until one reaches the switch, which may be in gas or transformer

oil. Somewhere near here the geometry is sufficiently distorted from the ideal conic that the TEM mode does not adequately describe the fields and there is a rise-time limitation associated with the transmission-line cross section dimensions at this position. In the switch itself there is also the problem of the arc characteristics such as inductance. For large voltages and currents one can use oil or pressurized SF_6 switches [117]. One can also look at silicon or gallium-arsenide optically triggered switches which are very fast [183], [186]. However, one may need arrays of these to switch the high voltages of interest.

Consider another approach to this risetime versus breakdown problem. Going back toward the conical apex one can stop on some surface with an acceptable electric field magnitude. Utilizing the electromagnetic uniqueness theorem one can specify the tangential electric field in the desired TEM mode on this cross section surface, perhaps a sphere (the significant portion thereof) or some other convenient surface [53]. Then if one can produce these fields on this surface the desired TEM wave will result. One way to do this is referred to as a distributed switch, in which a number of switches is distributed over the surface in a way which approximates the TEM mode when the switches close. The wavelength versus cross sectional limitation is replaced by the shorter wavelengths (faster times) associated with the switch spacing. Of course, the switch closing times and jitter need to be acceptably fast. Further improvement can be obtained by associating each switch with a wave launcher which transports the wave from the switch to the surface where all the subwaves come together to synthesize the TEM mode [63], [66]–[68], [103]. Note that the distributed-switch principle can be also used to increase the megavolts across the switch (for a given rise time) or attachment to a larger Marx generator, thereby allowing larger test volumes to be illuminated for specified field amplitudes.

An alternate approach to relaxing this rise-time limitation concerns the use of special kinds of lenses to transport the wave from a switch to the desired TEM mode without distortion. This involves concepts of differential geometry and transit-time and differential-impedance matching for every segment of the wavefront. These are summarized in a recent book with various geometries worked out, and a bibliography of the subject included [11]. In this concept, as one follows the TEM mode back toward the conical apex, one may wish to enter a high-dielectric-strength medium with relative permitivity (and perhaps relative permeability) greater than one (e.g., transformer oil). By appropriate shaping and variation of the constitutive parameters one can trace the wave back in a way which better matches to the switch configuration while minimizing dispersion and reflection. Of course the lens approach can be combined with the distributed switch, whether with a single lens, or separate lenses for individual switches or groups of switches.

While lightning simulators also have the purpose of producing large electromagnetic fields in the vicinity of the test object, the design requirements are significantly different [116]. While mechanical damage is associated

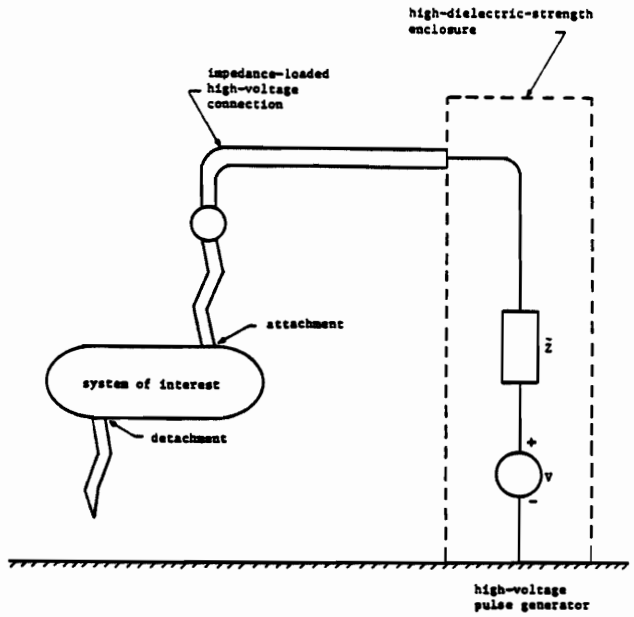

Fig. 11. Dual-arc lightning simulation.

with the large current (100 kA) and pulsewidth (10 s of μs), the electromagnetic interference (circuit upset and damage) is usually associated with higher frequency portions of the pulse (overall structure resonances, cable resonances, antenna and aperture coupling). In this context the distribution of the fields over the structure and in frequency content (or more general temporal content if nonlinearities are included) is quite important. A lightning simulator must adequately account for these phenomena if one is to have any confidence in the test results.

Briefly, much past work has been oriented toward driving such currents between attachment and detachment points (assumed) on the system [16(Clifford *et al.*, pp. 209–224)]. However, little attention has been given to the strong surface electric fields (of the order of air breakdown). For an aircraft this requires that the system be raised to a high potential (megavolts) with respect to other conductors in the vicinity. Furthermore, the lightning arc is a fundamental part of the interaction process, shifting the natural frequencies and associated modal surface-field distributions [15(Gardner *et al.*, pp. 491–533], [116]. An adequate simulation must address these phenomena.

There are various improvements that can be made in the design of lightning simulators for the electromagnetic interaction effects [116]. One can supplement the current (magnetic field) drive ("short circuit") by a voltage (electric field) drive ("open-circuit") in which the test object is taken to a different potential from the surroundings. By incorporating appropriate impedances and high-voltage switches in series with a capacitor bank one can modify the current drive to include some high voltage; some progress has been made in this direction [16(Clifford *et al.*, pp. 209–224)]. More generally, however, as indicated in Fig. 11 the simulator can attempt to produce an actual air arc attaching to and detaching from the test object as appropriate [116]. More work is needed in this direction.

In the subject of pulse power for driving EMP simulators (and related transient antennas) various things have been accomplished over the years. For the early years great credit is due to John C. (Charlie) Martin and his group at Atomic Weapons Establishment (Aldermaston, England) for the information developed on dielectric strength of various solids, liquids, and gases, and on fast switching, especially in transformer oil and SF_6. This is documented in the Dielectric Strength Notes and Switching Notes (as well as other series under Pulsed Electrical Power). In the U.S. this British influence has been important at the pulser manufacturers: Maxwell Laboratories, Physics International, and Pulse Sciences. In recent years there has been some updating in [117].

As pulse generators went to higher voltages with smaller rise times, they were no longer electrically small. A first improvement, using circuit concepts was that of a peaking capacitor C_p which is charged by the Marx generator with inductance L_M. If the Marx capacitance C_M is large compared to C_p and the peaking switch is fired when the Marx voltage is reached with

$$Z_L \simeq \left(\frac{L_M}{C_p}\right)^{1/2} \equiv \text{load impedance (high frequencies)} \quad (4.8)$$

then the rise is limited by the inductance of peaking switch [118]. Then the peaking capacitors were distributed in a form which made them part of the waveguiding structure (simulator antenna near the peaking switch), at least for high frequencies [119]–[121]. As discussed previously more modern research then goes on to the distributed switch and use of lenses for further improvements.

In the case of radiating HPM systems the optimum antenna is typical of microwave antennas with the additional requirement of very high fields which may cause breakdown [60], [62], [75], [80], [82], [124], [185]. For such an application reflector antennas are appropriate for their good directive and large-aperture properties. The waveguides and feeds will have to be designed with vacuum and/or SF_6 regions to handle the high fields, thereby incorporating some features of EMP simulators [64].

HPM sources involve extensions of the more common microwave sources to include the higher powers available from relativistic electron beams [17]–[20]. Already several GW of power (pulses of 100-ns order) have been obtained from single sources. Both magnetrons and vircators have delivered this power in standard rectangular waveguides where it can be appropriately utilized. Note that frequency ranges of interest here are from several hundred megahertz to several gigahertz. To go to higher powers it is desirable to understand how to use multiple sources. In this case the phases of the multiple signals need to be locked together, for which purpose symmetry in the source array is useful [122]. For this purpose it would be useful to have sources which operate in an amplifier-like mode so they can all be controlled from single master source. There is a promising source for this purpose which is klystron-like with the addition of a guiding magnetic field to hold together the bunching relativistic electron beam [20(Lau *et al.*, pp. 553–569)]. Work is needed on converting the modulated beam into microwave fields in a waveguide [123]. Obviously there is a lot of work needed on all aspects of the HPM source/radiation problem.

V. Interaction with Complex Electronic Systems

A. Interaction Description

The electromagnetic interaction problem is extremely complex. It is hard enough to calculate the fields on the exterior of a complex system such as a ship, missile, aircraft, tank, etc. This part of the problem shares a common application with radar cross sectional calculations. Going to the interior the complexity is typically very much greater. As computer codes have become more sophisticated and computers bigger and faster there is some hope of getting reliable surface currents and charges (apart from cases with air breakdown, etc.). As one goes to the interior and encounters thousands of wires going to numerous black boxes, antennas, etc., through various cavities and other strange structures the calculation problem gets quickly intractable. Even if one thought he could calculate such a complex problem, he would likely miss important signals because the system in the field is often different from the drawings by various changes for the convenience of the operators. So one has to consider what one can usefully do in this area.

In trying to tackle this difficult problem one needs to look for means of simplifying the problem so that something tractable and useful emerges. First observe the common nature of the interaction problem. For the most part the different environments (EMP, lightning, HPM) interact with complex systems in the same way. Since most of the problem can be thought of in the context of a linear, time-invariant system, for which the Laplace transform (complex frequency domain) is applicable, then the usual concepts of impedance and transfer function are appropriate. Frequency then is just a parameter in the interaction models and one uses the models most appropriate for the frequency regime of interest [3]. There are exceptions to this, in particular in the cases of nonlinearities associated with electrical breakdown. For example, in a direct lightning strike there is a lightning arc attached to the system and there may be corona surrounding antennas and apertures on the system exterior; even in this case one can generally use the linear analysis in the interior. Nonlinear protection devices (clamps, spark gaps, etc.) need special treatment if the signals are strong enough. The signals finally reach some circuit where there may be some kind of upset or even destruction of a circuit element (burnout). While this involves nonlinear processes one can use linear analysis (small signal theory) to estimate the signal levels at which failure (upset or burnout) will occur. One can refer to this concept as "linearity to failure" in the sense that linearity is approximately correct up until the time that the failure

occurs, after which the analysis is irrelevant for this purpose [90].

While the detailed response characteristics of complex systems are quite complicated some general trends can be summarized based on the various models of the processes involved (response of various elements organized by the EM topology) which, of course, has been developed from a lot of experience [3]. Referring to Fig. 12 we have the transfer function from an incident plane wave to some current or voltage on some interior terminal pair [62]. This can be thought of as the product T_0T_i of a transfer function to the exterior T_0 (for surface current or charge density) and a subsequent transfer function to the interior T_i. While there are exceptional cases, the typical or canonical system response can be divided into three bands with certain characteristic behavior.

The first band ($f < f_\ell$) is for frequencies for which the system is electrically small. In this region the response takes a derivative form (constant times $s = j\omega$) characteristic of electrically small antennas and voltage and current sources in transmission-line models for cables passing near apertures [3]. This assumes that the respective load impedances are neither zero nor infinite (i.e., are lossy). One can estimate f_ℓ based on the maximum linear dimensions of the system or the length of the associated cables (with some modification if reactive loads are involved.) For a large aircraft f_ℓ is a few megahertz. For a building such as a communication center with large mental appendages (power and communication conductors), f_ℓ can be considerably lower.

The second band ($f_\ell < f < f_h$) is the resonance region. Here the transfer function varies up and down as one passes through various resonances (poles in the complex frequency plane). Beginning with the lowest resonances associated with the major dimensions of the system (e.g., fuselage and wing lengths for an aircraft) and the interior electrical wiring (cable shields and internal wires) of similar length, one goes up through resonances associated with shorter wires and dimensions of interior cavities. Then there are dimensions of doors, windows, boxes for electronic equipment, spacing between hinges and rivets, etc. For typical systems the resonance region extends up to about a gigahertz, corresponding to half-or quarter-wave resonance to the smallest characteristic dimensions involved in the system construction, this coming from the smallest sizes with which human beings usually work, related to the size of one's hand.

Above this frequency (f_h) the transfer function rolls off. A simple model for this is that of a conductor parallel to a ground plane. Above the frequency where the spacing is a quarter wave length (assuming resistive termination of the resulting transmission line) the current on the conductor takes an approximate integral form (constant/s) [3]. There are other processes (such as attenuation on transmission lines in the gigahertz region) which also makes the response roll off above f_h.

It is hard to overemphasize the importance of resonances. These dominate the transient response, and it was

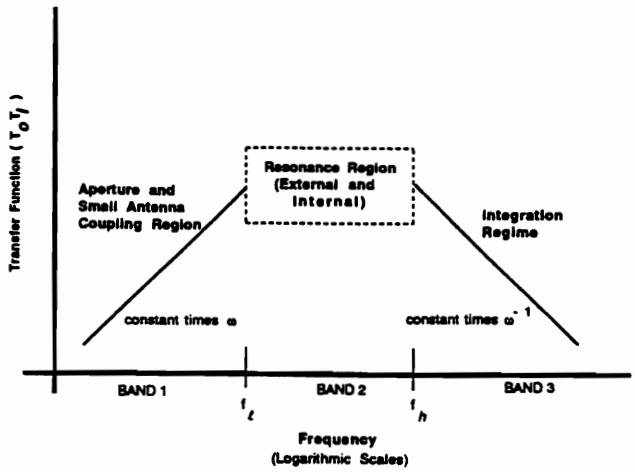

Fig. 12. Canonical system response as a function of frequency.

this observation that led to the development of SEM [2], [4(Baum, pp. 129–179)], [5], [145], [181]. While it may be difficult to calculate them a priori with any precision (particularly for some of the internal resonances), they are fundamental to understanding the unintentional ("back door") response of systems. For deliberate EM transmission and reception (communications, radar, etc.) of course one has considerable knowledge of their in-band characteristics, and the important frequencies can go much higher than a gigahertz (or much lower than a megahertz), so one has to understand Fig. 12 as a canonical case with exceptions allowed, especially for deliberate EM transmission and reception ("front door" response).

B. Interaction Maximization

Understanding something about the interaction processes and trends one can ask what to do with this. Suppose, on the one hand, one wishes to maximize the response of some system, i.e., get the biggest signals (in the sense of peak voltage, energy, etc.) to failure ports in the system. One can design a microwave system with this in mind.

For this purpose factor the transfer function from source to some port of interest in the system as indicated in Fig. 13 [62]. As discussed in [60], the appropriate type of antenna is one which fills up its aperture approximately uniformly in amplitude under an electrical breakdown (peak electric field) limitation so as to allow maximum power radiation. This is normally realized with the usual kind of reflector used in many microwave radars. With appropriate phase control on the aperture (focusing) one can obtain at some position $\vec{r}_o$ (perpendicular to antenna aperture)

$$\begin{aligned} E_f &= E_0 \frac{\omega_s A}{2\pi c r_0} = E_0 \frac{f_s A}{c r_0} = E_0 \frac{A}{\lambda_s r_0}, \\ r_0 &= |\vec{r}_0|, \quad A \equiv \text{antenna aperture area}, \\ E_0 &= \text{tangetial electric field strength on aperture}, \\ \omega_s &\equiv \text{source radian frequency}, \\ f_s &\equiv \text{source frequency}, \\ \lambda_s &\equiv \text{source wavelength}. \end{aligned} \tag{5.1}$$

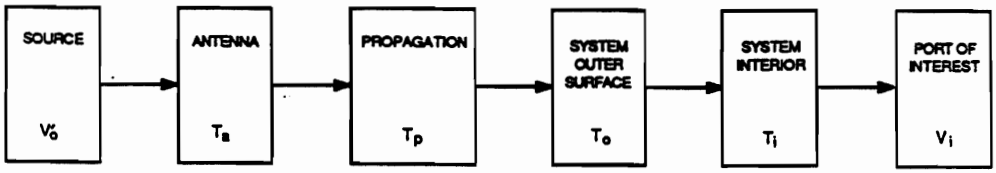

Fig. 13. Factorization of transfer function from source to system.

The average power (average over one cycle) is

$$P_{\text{avg}} = \frac{1}{2}\frac{A}{Z_0}E_0^2 = \frac{1}{2}\frac{V_0'^2}{Z_0}$$
$$V_0' \equiv \text{effective voltage of source.} \tag{5.2}$$

Note this effective voltage is not in general an actual voltage, in which an appropriate source impedance is needed. The antenna transfer function (to field incident on the system) is then (removing delay)

$$T_a \equiv \frac{E_f}{V_0'} = \frac{\omega_s A^{1/2}}{2\pi c r_c} = \frac{f_s A^{1/2}}{c r_c} = \frac{A^{1/2}}{\lambda_s r_0} \tag{5.3}$$

with dimensions m^{-1}.

In Fig. 13 there is allowed a transfer function T_p for distortion by the intervening medium; for present purposes this is set to one. Accumulating all the factors we have the response at a box input (more generally a failure port) as

$$\simeq V_0' \frac{f_s A^{1/2}}{c r_0} T_0 T_i. \tag{5.4}$$

This is appropriate if the basic limitation is the source V_0' (i.e., the source power). If the basic limitation is the electric field E_0 on the antenna aperture we have another form as

$$V_i \simeq E_0 \frac{f_s A}{c r_0} T_0 T_i. \tag{5.5}$$

In both cases we have a simple analytical expression followed by the factor $T_0 T_i$ which has been summarized graphically for our canonical system in Fig. 12.

Considering the peak signal V_i (or ∞-norm), let the incident pulsewidth be large enough that the selected system resonance has time to "ring up" and achieve a quasi-CW value [96]. Note that in general V_i is increased by increasing f_s, except that above f_h the factor $T_0 T_i$ counteracts this increase. Furthermore as frequency is increased V_0' generally decreases. Roughly speaking this says that f_s can be best chosen as around f_h, and tuned to a convenient resonance near there. If the basic limitation is V_0' then the rate of decrease of V_0' with frequency determines whether f_s should be near f_h or somewhat lower. Note in both (5.4) and (5.5) that increasing A also helps.

If another aspect of the signal such as energy delivered to the failure port (related to 2-norm) is the parameter of interest then pulsewidth is also important. If the complex source frequency (for a damped sinusoid) is $s_s = \Omega_s + j\omega_s$, then $|\Omega_s|^{-1}$ is the decay time constant of the pulse, the energy in the incident pulse being proportional to this, as is the received energy provided $|\Omega_s|$ is smaller than the width of the system resonance (also centered on ω_s).

C. Interaction Organization and Control

Another use of an understanding of interaction processes is the control of this interaction in the system design or hardening. However, first we need an organized format to put some order into this process. For a modern complex electronic system the large number of elements (wires, apertures, boxes, etc.) to be considered gives great importance to ways to reduce this number to a more tractable set of important elements. The major concept in this regard is EM topology. First, however, consider the description of transmission-line networks which will give us an understanding of some of the requisite concepts.

1) Multiconductor Transmission Lines: As indicated in Fig. 14 we have a set of junctions denoted by J_v which can be thought of as general N-port networks representing "black boxes" in some system. These junctions are joined by tubes denoted by $T_{v,v'}$, joining J_v and $J_{v'}$ (with a superscript if needed for more than one such tube). Each tube contains some number of wires (plus reference) and there are two vector waves (or N-waves) W_u (for two values of u) denoting the two directions of propagation on each tube. These waves are the important variables for which we define

$$N_u \equiv \text{number of wires for } u\text{th wave}$$
$$x_u \equiv \text{coordinate (meters) for } u\text{th wave propagation from 0 to } L_u \text{ (length of tube)}$$
$$\left(\tilde{Z}_{c_{n,m}}(s)\right)_{u,u} \equiv \text{characteristic impedance matrix } (N_u \times N_u) \text{ for } u\text{th wave}$$
$$\left(\tilde{V}_n(x_u s)\right)_u \equiv \left(\tilde{V}_n(x_u, s)\right) + \left(\tilde{Z}_{c_{n,m}}(s)\right)_{u,u} \cdot \left(\tilde{I}_n(x_u, s)\right)$$
$$\equiv \text{combined voltage wave vector (containing voltage and current) propagating in } x_u \text{ direction (direction of positive current)}$$
$$\left(\tilde{V}_{s_n}'(x_u, s)\right)_u \equiv \left(\tilde{V}_{s_n}'(x_u, s)\right) + \left(\tilde{Z}_{c_{n,m}}(x_u, s)\right) \cdot \left(\tilde{I}_{s_n}'(x_u, s)\right)$$
$$\equiv \text{combined per-unit-length source vector containing longitudinal voltage source (positive in } x_u \text{ direction) and transverse current source} \tag{5.6}$$

Combined with

$$\left(\tilde{S}_{n,m}(s)\right)_{u,v} \equiv \text{scattering matrix } (N_u \times N_v)$$

scattering vth wave into uth wave at junction with $x_v = L_v,\ x_u = 0$

$$\left(\tilde{\Gamma}_{n,m}(s)\right)_{u,v} = \begin{cases} \exp(-(\tilde{\gamma}_{c_{n,m}}(s))_u L) & \text{for } u = v \\ 0 & \text{for } u \neq v \end{cases}$$

$\equiv$ propagation matrix

$$(\tilde{\gamma}_{c_{n,m}}(s))_u = \left[\left(\tilde{Z}'_{n,m}(s)\right)_u \cdot \left(\tilde{Y}'_{n,m}(s)\right)_u\right]^{1/2}$$

(positive real (p.r.) square root)

$$\left(\tilde{Z}'_{n,m}(s)\right)_u \equiv \text{longitudinal impedance-per-unit-length matrix } (N_u \times N_u) \text{ on tube with } u\text{th wave}$$

$$\left(\tilde{Y}'_{n,m}(s)\right)_u = \text{transverse admittance-per-unit-length matrix } (N_u \times N_u) \text{ on tube with } u\text{th wave}$$

$$\left(\tilde{Z}_{c_{n,m}}(s)\right)_{u,u} = (\tilde{\gamma}_{c_{n,m}}(s))_u \cdot \left(\tilde{Y}'_{c_{n,m}}(s)\right)_u^{-1} = (\tilde{\gamma}_{c_{n,m}}(s))_u^{-1} \cdot \left(\tilde{Z}'_{n,m}(s)\right)_u$$

$$\left(\tilde{\Lambda}_{n,m}(x'_u s;(\cdot))\right)_{u,v} = \begin{cases} \int_0^{L_u} \exp\left(-(\tilde{\gamma}_{c_{n,m}}(s))_u [L_u - x'_u]\right) (\cdot)\, dx'_u & \text{for } u = v \\ 0 & \text{for } u \neq v \end{cases}$$

$= N_u \times N_u$ matrix operator (on operand denoted by $(\cdot)$).

(5.7)

These are put together in the BLT equation [8(Baum, pp. 467–547)] as

$$\left[\left((1_{n,m})_{u,v}\right) - \left(\left(\tilde{S}_{n,m}(s)\right)_{u,v}\right) \odot \left(\left(\tilde{\Gamma}_{n,m}(s)\right)_{u,v}\right)\right] \odot \left(\left(\tilde{V}_n(0,s)\right)_u\right) = \left(\left(\tilde{S}_{n,m}(s)\right)_{u,v}\right) \odot \left(\left(\tilde{V}_{s_n}(0,s)\right)_u\right)$$

$$\left(\left(\tilde{V}_{s_n}(s)\right)_u\right) = \left(\tilde{\Lambda}_{n,m}(x'_u, s;(\cdot))_{u,v}\right) \odot \left(\left(\tilde{V}'_{s_n}(x'_u, s)\right)_u\right)$$

$\equiv$ source supervector

$$\left(\tilde{V}_{s_n}(s)\right)_u = \int_0^{L_u} \exp\left(-(\tilde{\gamma}_{c_{n,m}}(s))_u [L_u - x'_u]\right) \cdot \left(\tilde{V}'_{s_n}(x'_u, s)\right)_u dx'_u$$

$\equiv$ source vector for uth wave. (5.8)

Note the use of supervectors and supermatrices (or divectors and dimatrices in this case) in which each vector or matrix has been partitioned into blocks (denoted by dummy u, v indices) with generalized dot product $\odot$. The individual blocks have dummy indices n, m. This partitioning can be carried out to as many levels (or sets of dummy indices) as desired. Having found the solutions for the supervector waves leaving each junction voltages and currents are straight forwardly constructed everywhere.

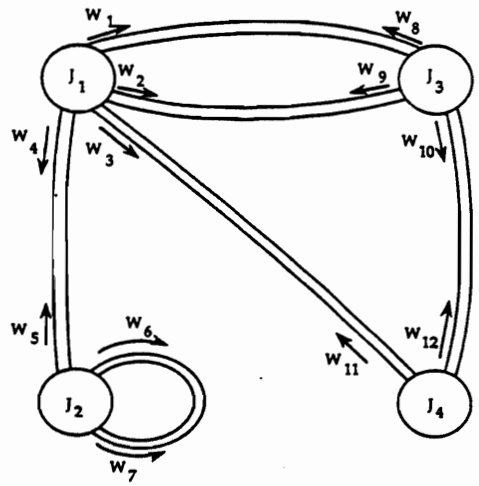

Fig. 14. Transmission-line graph.

The BLT equation is a formal way to express the signals on an entire transmission-line network, the solution being found by inversion of a supermatrix [95]. In time domain the supermatrices are also convolution operators. An example problem involving three waves (on two tubes) applying to a Marx generator with peaking-capacitor arms have been worked in [121]. Here the solution was also easily expressible in time domain due to the frequency-independent modal velocities associated with frequency-independent inductance- and capacitance-per-unit-length matrices.

While concerned with multiconductor transmission lines some other observations are appropriate. Some recent progress has been made on the theory of nonuniform tubes, i.e., the per-unit-length impedance and admittance matrices being allowed to be a function of position x. In [101] perturbation theory (as in quantum mechanics) is applied to small variations to find splitting of degenerate natural frequencies. In [97] a high-frequency approximation is found (say for waves propagating in the $+x$ direction) providing all modes have the same propagation constant as

$$(\tilde{\gamma}_{c_{n,m}}(s)) = \tilde{\gamma}(1_{n,m})$$

$$\left(\tilde{V}_n(x,s)\right) = \exp(-\tilde{\gamma}_z)(\phi_{n,m}(x)) \cdot \left(\tilde{V}_n(o,s)\right) \quad \text{as} \quad s \to \infty$$

$$\frac{d}{dx}(\phi_{n,m}(x)) = \left\{-\frac{1}{2}(Z_{c_{n,m}}(x)) \cdot \frac{d}{dx}(Y_{c_{n,m}}(x))\right\} \cdot (\phi_{n,m}(x))$$

$$(\phi_{n,m}(0)) = (1_{n,m})$$

$$(Y_{c_{n,m}}(x)) = (Z_{c_{n,m}}(x))^{-1}$$

$\equiv$ characteristic admittance matrix

(5.9)

where the characteristic impedance matrix has been assumed frequency independent in the high-frequency limit (e.g., perfectly conducting wires in a lossless perfectly conducting medium). This gives a vector/matrix generalization of the WKB equation. A normalized form of this equation can be found from

$$\begin{aligned}
&\left(z_{c_{n,m}}(x)\right) \equiv \left(Z_{c_{n,m}}(x)\right)^{1/2} \\
&\left(y_{c_{n,m}}(x)\right) \equiv \left(Y_{c_{n,m}}(x)\right)^{1/2} = \left(z_{c_{n,m}}(x)\right)^{-1} \\
&\left(\Phi_{n,m}(x)\right) \equiv \left(y_{c_{n,m}}(x)\right) \cdot \left(\phi_{n,m}(x)\right) \cdot \left(z_{c_{n,m}}(x)\right) \quad (5.10)
\end{aligned}$$

where the p.r. square root is used (p.r. eigenvalues). Note that a sufficient condition for diagonalizability is that the matrix be a complex number (say s) times a real symmetric matrix (inductance- and capacitance-per-unit-length matrices) [102]. We then obtain

$$\begin{aligned}
&\frac{d}{dx}\left(\phi_{n,m}(x)\right) = \left(C_{n,m}(x)\right) \cdot \left(\phi_{n,m}(x)\right) \\
&\left(C_{n,m}(x)\right) = \frac{1}{2}\left(y_{c_{n,m}}(x)\right) \cdot \frac{d}{dx}\left(z_{c_{n,m}}(x)\right) \\
&\qquad - \frac{1}{2}\left[\frac{d}{dx}\left(z_{c_{n,m}}(x)\right)\right] \cdot \left(y_{c_{n,m}}(x)\right) \\
&\qquad = -\left(C_{n,m}(x)\right)^{T} \quad \text{(skew symmetric)} \\
&\left(\Phi_{n,m}(0)\right) = \left(1_{n,m}\right). \qquad (5.11)
\end{aligned}$$

The equations for $(\phi_{n,m}(x))$ and $(\Phi_{n,m}(x))$ give rise to a solution known as the matrizant which has an infinite series representation where the nth term is the nth repeated integral of the coefficient matrix. Closed form solutions are obtained in special cases for which case the equation for $(\Phi_{n,m}(x))$ is more useful due to the constraints on $(C_{n,m}(x))$. If the coefficient matrix can be written as a sum of scalar functions of x times constant matrices, all pairs of these matrices commuting, then we have

$$\begin{aligned}
&\left(C_{n,m}(x)\right) = \sum_{p=1}^{P} h_p(x)\left(c_{n,m}\right)_p \\
&\left(c_{n,m}\right)_{p_1} \cdot \left(c_{n,m}\right)_{p_2} = \left(c_{n,m}\right)_{p_2} \cdot \left(c_{n,m}\right)_{p_1} \quad \text{for all } p_1, p_2 \\
&\left(\Phi_{n,m}(x)\right) = \exp \int_0^x \left(C_{n,m}(x')\right) dx' \\
&\qquad = \exp \sum_{p=1}^{P} g_p(x)\left(c_{n,m}\right)_p \\
&\qquad = \bigodot_{p=1}^{P} \exp g_p(x)\left(c_{n,m}\right)_p \\
&g_p(x) = \int_0^x h_p(x')\, dx' \qquad (5.12)
\end{aligned}$$

as the general solution. Due to the special normalized form of this coefficient matrix we also have

$$\det[(\Phi_{n,m}(x))] = 1. \qquad (5.13)$$

Considering different dimensions N of these $N \times N$ matrices we have the well known scalar solution ($\Phi = 1$) for $N = 1$. For $N = 2$ the fact that there is only one independent element $h(x)$ for the skew symmetric coefficient matrix allows such cases now to be solved by quadrature, and various examples have been worked out [63], [67], [68]. Cases with higher N can also be worked out, at least within the above-stated sufficient conditions.

Another approach to the nonuniform tube involves the assumption of commutativity of $\left(\tilde{Z}'_{n,m}(x,s)\right)$ and $\left(\tilde{Y}'_{n,m}(x,s)\right)$. This allows (with reciprocity) the complete diagonalization of the telegrapher equations resulting in N scalar equation for the eigenvalues [102]. A special case involves circulant matrices which arise in certain problems including cases of rotation symmetry (N-fold rotation axis) [103]. The special forms of x-variation (linear, exponential, etc.) which result in analytic solutions now generalize to $N > 1$ and complete solutions (all frequencies) can be obtained.

2) Electromagnetic Topology: The fundamental organizing principle is EM topology [3], [86], [87], [180]. This includes a qualitative (or descriptive) aspect as well as a quantitative aspect. Furthermore the quantitative aspect can be simplified by the use of bounds, especially those given by norms. See [10] for a more complete bibliography, and [6] for a collection of papers (special issue).

In qualitative (or discrete) form divide three-dimensional Euclidean space into a set of volumes V_n with boundaries $S_{n,m}$ between adjacent volumes. This EM topology has a graphical representation (the interaction sequence diagram) in which the volumes are represented by vertices (or nodes) and the boundaries by edges (or branches) connecting the associated node pairs. More important is the additional ordering imposed by a hierarchical EM topology as indicated in Fig. 15. In this concept we think of a nested set of surfaces (shields) separating volumes (layers) with layer index λ (beginning with one for the outermost volume). Then besides such a "series" decomposition we can have a "parallel" decomposition by definition of sublayers $V_{\lambda,\ell}$ and associated subshields $S_{\lambda,\ell_1;\lambda+1,\ell_2}$ with sublayer index ℓ. Note in Fig. 15 that the interaction sequence diagram is now a tree graph which has the property that there is a unique path connecting any pair of sublayers. Along this path connecting V_{λ_1,ℓ_1} to V_{λ_2,ℓ_2} the path crosses a number of subshields (an integer) known as the relative shielding order $R_{\lambda_1,\ell_1;\lambda_2,\ell_2}$ [88]. This latter can be used to define a matrix of such integers for primary sublayers (those containing equipment to be protected or interference from sources to be kept in) from which one can construct an EM topology for some system design.

Such concepts can be applied at this point to the construction of expert computer programs for organizing a system EM topology and an appropriate set of transfer functions [6(Messier, pp. 79–93)], [149], [172]. These concepts are being implemented in the design of military systems as seen in a new MIL-STD [178] with other related documents in preparation. For groundbased C^{4}I systems the emphasis is on a single shield surface with a minimum number of penetrations (all controlled, with no penetrating ground wires) as a low-risk hardening approach. For aerospace

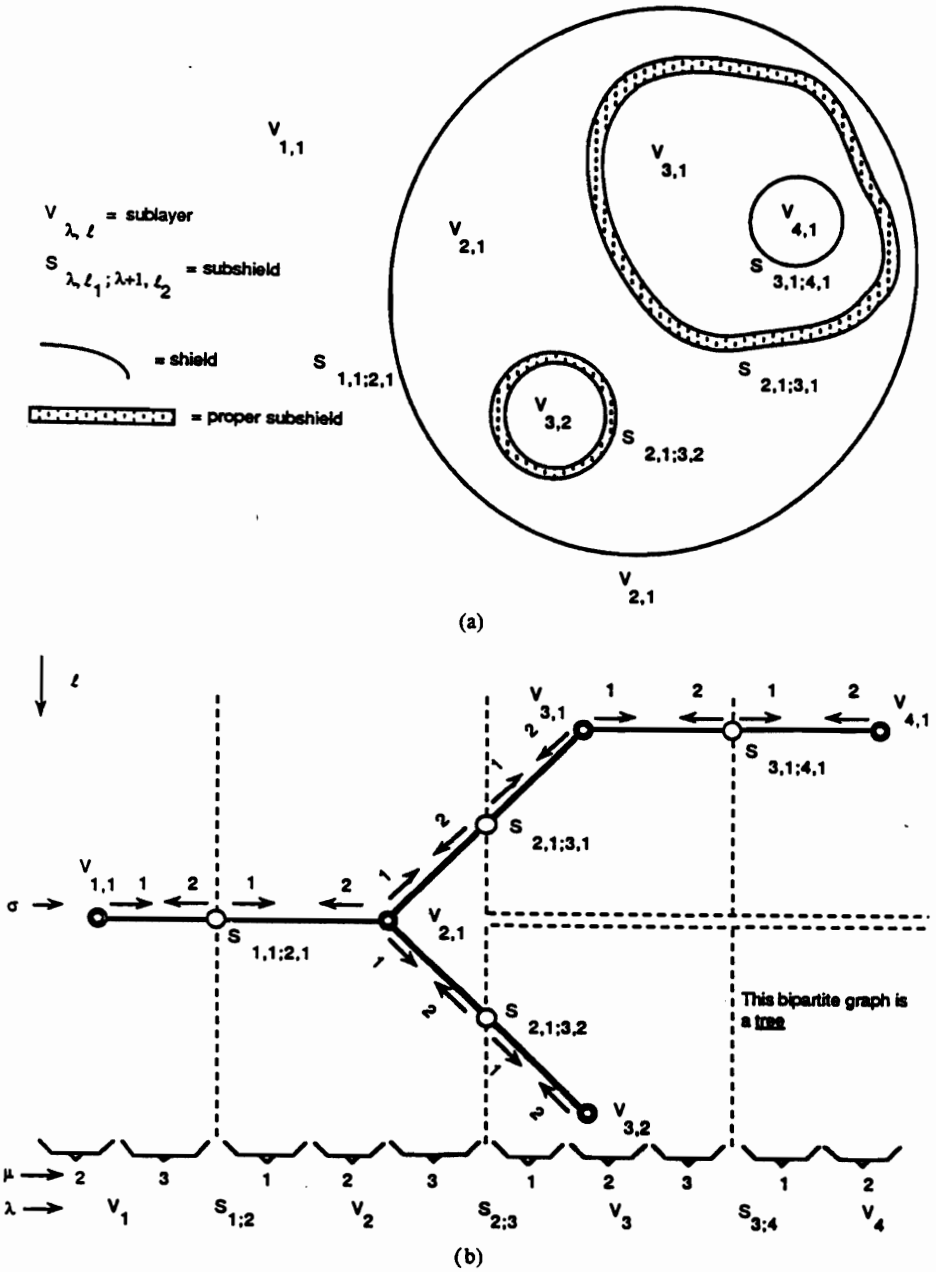

Fig. 15. Sublayers and subshields in hierarchical topology. (a) Volume / surface topology. (b) Interaction sequence diagram.

vehicles the topology may involve multiple shields (nested) with the attenuation appropriately allocated [88].

Not let us apply the BLT equation (5.8) for multiconductor transmission-line networks to our EM topology. Since this equation is written on a graph let us compare such a graph (Fig. 14) to the interaction sequence diagram (Fig. 15) with decomposition to sublayer level. Identifying junctions with sublayers and tubes with subshields the BLT equation can be applied to the EM topology in the form

$$\left(\left(\left(\tilde{I}_{n,m}(s)\right)_{w,w'}\right)_{\lambda,\lambda'}\right) \odot \left(\left(\left(\tilde{V}_n(s)\right)_w\right)_\lambda\right) = \left(\left(\left(\tilde{V}_n^{(s)}(s)\right)_w\right)_\lambda\right)$$

$$\left(\left(\left(\tilde{I}_{n,m}(s)\right)_{w,w'}\right)_{\lambda,\lambda'}\right) = \left(\left((1_{n,m})_{w,w'}\right)_{\lambda,\lambda'}\right) - \left(\left(\left(\tilde{S}_{n,m}(s)\right)_{w,w'}\right)_{\lambda,\lambda'}\right) \equiv \text{interaction supermatrix} \tag{5.14}$$

where w represents a set of topological indices, including ℓ (sublayers), μ (layer part for coupling (sources in layer), propagation, and penetration (going to next layer) as indicated in Fig. 15(b) [3]), and other indices which need not concern us here. Note that the propagation matrix has gone away as we have shrunk the tube lengths to zero.

Furthermore the new source voltages are found from (5.8) by replacing the distributed per-unit-length source vector by a discrete source, integrating over this with the matrix operator (now an identity), and multiplying by the scattering supermatrix. With the tubes at zero length we can choose each characteristic impedance matrix for our convenience, say as a resistance R times an identity matrix. The volumes (layers, etc.) are modelled as N-port networks for purpose of defining the scattering supermatrix.

At this point the theory can be implemented as a general calculational technique in which one must first specify the topology and then the various matrix blocks and source vectors, whether from a mathematical model (analytical or numerical) or from experimental data. This is being actively pursued by French groups with the CRIPTE computer code which has the flexibility of allowing both multiconductor transmission-line (5.8) and electromagnetic (5.14) forms in various combinations [150], [151], [177]. The agreement with experimental data [177] is quite good and represents a significant improvement in the accuracy and complexity of electromagnetic geometry that can be treated for the internal interaction problem.

In the form of (5.14) we can now consider the good-shielding approximation. Consider the blocks (first level) of the interaction supermatrix $\left((\tilde{I}_{n,m}(s))_{w,w'}\right)_{\lambda,\lambda'}$. For $|\lambda - \lambda'| \geq 2$ these are zero supermatrices, reflecting the fact that signals do not connect directly between nonadjacent sublayers (relative shielding order ≥ 2), but rather have to propagate through intermediate sublayers, a consequence of the ordering in the hierarchical topology. Then assume that the off-diagonal blocks $(|\lambda - \lambda'| = 1)$ are in some sense (a norm sense) small compared to the diagonal blocks. Furthermore let (all sources outside)

$$\left(\left(\tilde{V}_n^{(s)}(s)\right)_w\right)_\lambda = ((0_n)_w) \quad \text{for} \quad \lambda > 1. \tag{5.15}$$

Then by Gaussian elimination in (5.14) with supervector unknowns and supermatrix coefficients we obtain the approximate solution [87], [94]

$$\begin{aligned}\left(\left(\tilde{V}_n(s)\right)_w\right)_\lambda \simeq \Bigg\{\bigodot_{\lambda'=0}^{\lambda-2}\Bigg[\left(\left(\tilde{S}_{n,m}(s)\right)_{w,w'}\right)_{\lambda-\lambda',\lambda-\lambda'} \\ \bigodot\left(\left(\tilde{S}_{n,m}(s)\right)_{w,w'}\right)_{\lambda-\lambda',\lambda-1-\lambda'}\Bigg]\Bigg\} \\ \bigodot\left(\left(\tilde{V}_n^{(s)}(s)\right)_w\right)_1\end{aligned} \tag{5.16}$$

where as discussed in [94] this simple form is based on the assumption that signals in the sublayers are terminated by R at the subshields (no "reflections"), other similar forms being available if this condition is not met.

The important thing is the form of (5.16) as a continued product giving the signals in the λth layer as a product of the exterior ($\lambda = 1$) sources times transfer functions (in the form of scattering supermatrices) for each topological entity (subshield, sublayer) encountered in the interaction sequence diagram in passing from $\lambda = 1$ to the λ of interest. Further simplifying (5.16) by the use of norms and neglecting the transmission through the sublayers (assuming it is bounded by one by passivity) gives

$$\begin{aligned}\left\|\left(\left(\tilde{V}_n(s)\right)_w\right)_\lambda\right\| \lesssim \left\{\prod_{\lambda'=0}^{\lambda-2}\left\|(S_{n,m}(s))_{\lambda-\lambda',\lambda-1-\lambda'}\right\|\right\} \\ \cdot\left\|\left(\left(\tilde{V}_n(s)\right)_w\right)_1\right\|.\end{aligned} \tag{5.17}$$

These norms are all real nonnegative scalars. So our problem is reduced to a set of scalars, one for each subshield, these scalars defining shielding effectiveness (in a bounding sense) for each subshield. Note that while (5.16) is here written in frequency domain, it can be applied in time domain as well by use of convolution (and associated norms). Furthermore, while we have been considering the signals as propagating from $\lambda = 1$ as the "outside," the signals (interference) can originate in any sublayer, and the above formulas apply to this case as well by reindexing the subshields as though this sublayer were the "outside." This is related to the concept of topological inversion [88].

3) Norms: Now consider the use of norms for bounding signal response [90], [98], [113]. These are appearing in specification and standards [178] as a way of simplifying the consideration of the complicated waveforms typically encountered. Vector norms are defined by the properties

$$\begin{aligned}\|(u_n)\| = 0 \quad \text{iff} \quad (u_n) = (0_n) \\ \|\nu(u_n)\| = |\nu|\,\|(u_n)\| \\ \|(u_n) + (v_n)\| \leq \|(u_n)\| + \|(v_n)\|, \quad \|(u_n)\| \\ \text{depends continuously on } (u_n).\end{aligned} \tag{5.18}$$

Associated matrix norms are defined by

$$\|(A_{n,m})\| \equiv \sup_{(u_n)\neq(0_n)} \frac{\|(A_{n,m})\cdot(u_n)\|}{\|(u_n)\|} \tag{5.19}$$

and have the additional product inequality:

$$\|(A_{n,m})\cdot(B_{n,m})\| \leq \|(A_{n,m})\|\,\|(B_{n,m})\|. \tag{5.20}$$

The common p-norm has for N-component vectors

$$\|(u_n)\|_p \equiv \left\{\sum_{n=1}^{N}|u_n|^p\right\}^{1/p}, \qquad \|(u_n)\|_\infty = \max_n |u_n| \tag{5.21}$$

and for $N \times M$ matrices in special cases:

$$\begin{aligned}\|(A_{n,m})\|_1 &= \max_{1\leq m\leq M}\sum_{n=1}^{N}|A_{n,m}| \\ \|(A_{n,m})\|_\infty &= \max_{1\leq m\leq N}\sum_{m=1}^{M}|A_{n,m}| \\ \|(A_{n,m})\|_2 &= \left[\chi_{\max}\left((A_{n,m})^\dagger\cdot(A_{n,m})\right)\right]^{1/2} \\ \chi_{\max} &\equiv \text{maximum eigenvalue.}\end{aligned} \tag{5.22}$$

For time domain we need function norms with the properties:

$$\|f(t)\| = 0 \quad \text{iff} \quad f(t) = 0 \quad \text{(measure sense)},$$
$$\|\nu f(t)\| = |\nu| \, \|f(t)\|$$
$$\|f_1(t) + f_2(t)\| \le \|f_1(t)\| + \|f_2(t)\|. \tag{5.23}$$

Operator norms are defined by

$$\|\Lambda(\,)\| \equiv \sup_{\|f(t)\| \neq 0} \frac{\|\Lambda(f(t))\|}{\|f(t)\|} \tag{5.24}$$

and have the additional product inequality:

$$\|\Lambda(Y(\,))\| \le \|\Lambda(\,)\| \, \|Y(\,)\|. \tag{5.25}$$

For the p-norm summation is replaced by integration as

$$\|f(t)\|_p \equiv \left\{ \int_{-\infty}^{\infty} |f(t)|^p \right\}^{1/2}$$
$$\|f(t)\|_\infty = \sup_t |f(t)|. \tag{5.26}$$

For our purposes the important operator is convolution as $g(t)o$ with

$$F(t) = g(t)o\, f(t), \qquad \tilde{F}(s) = \tilde{g}(s)\, \tilde{f}(s). \tag{5.27}$$

For causal $g(t)o$ we have [113]

$$\|g(t)o\| \le \|g(t)\|_1, \qquad \text{for} \quad 1 \le p \le \infty$$
$$\text{with equality for } p = 1, \infty. \tag{5.28}$$

For the two-norm we have

$$\|f(t)\|_2 = \frac{1}{\sqrt{2\pi}} \left\| \tilde{f}(j\omega) \right\|_2$$
$$\|g(t)o\| = |\tilde{g}(j\omega)|_{\max} \le \|g(t)\|_1. \tag{5.29}$$

In applying the norms to bounding the transfer of signals through subshields, note that in time domain we have a vector of time-domain functions so that both summation and integration are used. For the p-norm we have

$$\|(V_n(t))\|_p = \left\| \|(V_n(t))\|_{pv} \right\|_{pf}$$
$$= \left\| \left(\|V_n(t)\|_{pf} \right) \right\| \tag{5.30}$$

where a subscript v denotes vector (or matrix) sense and f denotes function (or operator) sense. Let the matrix convolution operator take the form

$$\left(V_n^{(\text{out})}(t) \right) = (T_{n,m}(t))^o \left(V_n^{(\text{in})}(t) \right) \tag{5.31}$$

where the superscript "out" indicates the signals penetrating through the subshield. For the important case of nonlinear protection devices define a norm limiter (with value X_n and a given selected norm) via

$$\left\| V_n^{(\text{out})}(t) \right\| \le X_n \tag{5.32}$$

for a diagonal transfer-function matrix, no matter what $V_n^{(\text{in})}(t)$ is. An ideal norm limiter would not affect $V_n^{(\text{out})}$ (as influenced by $T_{n,n}(t)o$) until after the time that the norm-limiting value is reached. Examples include ideal clamps and fuzes with appropriate filters to absorb reflections. Combining the norm-limiters with two diagonal transfer-function matrix convolution operators (one before (superscript 1) and one after (superscript 2)) gives [98] (see (5.33) on the bottom of the page). The bound for shielding effectiveness of a subshield now includes both linear filters and nonlinear protection devices.

So finally we have a formula, written on an EM topology, which reduces the system response to a set of norms (bounds) associated with the subshields of the system. Furthermore, the parameters in this formula are concerned with only a small portion of the system elements, i.e., excluding the system functional equipment in the sublayers. Turning this around it allows one to specify the signal norms in the various sublayers and use this to design the required characteristics of the subshields.

VI. System Testing/Assessment

Now we consider the hardest part of the HPE problem. How does one determine the effects on actual complex electrical systems? This involves several questions and some not-so-easy answers.

A. What Does it Mean for a System to Survive a Given Environment?

This question is more subtle than it may seem. What does it mean to survive? This could mean 1) not immediately totally destroyed, 2) can be repaired to function again at some future date, 3) not prevented from accomplishing its mission, or 4) not be affected in any noticeable way. For example, if an aircraft is struck by lightning the basic design criterion might be that it can safely land (on an emergency basis if necessary). The fact that some radio has been made inoperative may be acceptable. On the other hand, for a military aircraft exposed to a nuclear EMP (or HPM) it may be important that it continue to carry out its mission unimpaired (e.g., weapons on target) for which case the functioning of various pieces of electronic equipment may be very important.

$$\left\| \left(V_n^{(\text{out})}(t) \right) \right\|_p \le \left\| \left(\left\| T_{n,n}^{(2)}(t) \right\|_{pf} \left\{ \text{lesser of} \left[X_n, \left\| T_{n,n}^{(1)}(t) \right\|_{pf} \left\| V_n^{(\text{in})}(t) \right\|_{pf} \right] \right\} \right) \right\|_{pv}$$
$$\le \left\| \left(\left\| T_{n,n}^{(2)}(t) \right\|_{1f} \left\{ \text{lesser of} \left[X_n, \left\| T_{n,n}^{(1)}(t) \right\|_{1f} \left\| V_n^{(\text{in})}(t) \right\|_{1f} \right] \right\} \right) \right\|_{pv}. \tag{5.33}$$

One then needs to consider the system, its mission, and the environment of concern (including likelihood of exposure) in order to define an appropriate *criterion* for survival in these contexts. Section II discusses the various environments, but there is more to this than just a specified environment.

B. How Does one Know that a System will Survive a Given Environment?

The basic answer to this question is to operate the system in this environment and see if it survives as in Section VI-A. This is sometimes actually possible to determine. If, for example, some electronic system has an EMC problem in its normal operational environment, it will malfunction (not be able to communicate or whatever) and the fact of this problem will be evident to the operators. In severe cases an aircraft might even crash. Consider a flying aircraft being struck by lightning. If over a sufficient period of time the fleet of a particular aircraft model (all identical) receive some large number of strikes one need only review the data of number of crashes, equipment requiring repair, etc., to determine survival (per Section VI-A). In this case one can even make probabilistic statements concerning survival.

It would be preferable to be able to determine the system survivability without having to accept the consequences of vulnerability (not functional systems, crashes, etc.) before one builds a large number of such systems. So, while full operation in the environment of concern is the ultimate test, one would like to have some test which, if passed, would imply survival in the real operational environment. Furthermore, there are some systems with wartime missions for which the relevant environment is only present during war (e.g., the high-altitude EMP). The systems are required to be ready for a war which hopefully never comes, but if it comes, it is in general too late to fix (harden) the system.

So it is really necessary to address the question of determining system survivability some other way than exposure to the real environment before exposure to this real environment. Some may wish to determine survivability by analysis of the electromagnetic interaction, and while analysis is useful in understanding this process, experience has shown that it is unreliable for a vulnerability assessment in the case of a complex system. There are just too many variables and one does not *a priori* understand which are all the important ones. (See Section V.) Except in (rare) extremely simple cases with large safety margin one should not rely on such analysis.

This brings us to what kind of test (experiment) one can do and what kind is optimum. With what kind of an electromagnetic environment is the system to be excited, how is the system configured, and what is to be measured? While one can imagine using an arbitrary stimulus (an electromagnetic "hammer"), what does this accomplish besides expending money and time? One might discover one or more significant interaction paths into the system, and even harden them to some extent. However, how does one know if *all* the relevant interaction paths have been discovered? Furthermore, are all the signal strengths that may cause failure in the system as large as they would be in the real environment? There are so many potential signals of interest (voltages/currents at ports into electronic boxes/circuits) that for complex electronic systems one can only measure a small fraction of these in a practical test. (This can perhaps be improved by the use of special norm detectors [112].) In some cases there may be only a few relevant interaction paths to consider, but in general one does not know this *a priori.*

In order to make the test results relatable to the response in the real environment one needs a simulation (physical, not mathematical) of the real environment. As discussed in Section IV, simulators come in various kinds for the various environments and can be used in pulse and CW (using Fourier synthesis) modes of operation.

C. "Complete-Simulation" Test

By this is meant that the test is conducted in a way that the system reacts to the simulation environment in the same way and to the same degree as in the real operational environment. This sometimes referred to as a "threat-level" test, but there is much more than environmental "level" involved.

First, considering the environment itself, the incident fields (as in an EMP simulator) should have the same spatio-temporal distribution as the real environment. In the spatial context one often thinks of plane waves which in real simulators are not perfectly uniform. Some simulators also include a ground-reflected wave. The temporal content is *not* just a peak, rise time, and width. The frequency content (Fourier spectrum) is also very important due to the frequency-selective character (external and internal resonances) of the system. It is quite possible (and sometimes occurs) that the environment spectrum has various "notches" due to the pulser and/or simulator structure (antenna). As discussed in [96], this leads to severe undertesting when such notches coincide with system resonances. Furthermore, such notches are not always immediately obvious in the time-domain waveform.

Second, the introduction of the system in the proximity of the simulator should result in an interaction with the environment, the same as in the real operational situation. Specifically, the presence of the system can scatter fields which in turn scatter from the simulator back to the system, and so on in a multiple-scattering sense. This phenomenon is referred to as simulator/test-object interaction [1(Baum, pp. 35–53)], and it can in effect change the Green's function of the system. It is avoided by having the simulator sufficiently large compared to the test object, or sufficiently far from it. Since EMP simulators are generally open structures, radiation damping of the test-object (as well as simulator) aids in reducing this problem, thereby avoiding a "microwave-oven" effect.

Lightning simulators for direct strike electromagnetic interaction are somewhat different from EMP simulators in that there is no simple incident-field/scattered-field separation. As such the criterion environment must include the presence of the test object, attachment and detachment

points, arc resistances and geometry, currents, changes, etc. This is a considerable more complex problem. Of course, one can in some cases (e.g., aircraft) take the system to the *real* environment.

In the high-power microwave context this class of simulation is basically the real environment (plane wave, field strength, frequency, pulsewidth) except that one can use lower power sources by bringing the test object closer to the radiating source. Note, however, that the simulator/test-object interaction can be minimized by configuring the test object in its operational configuration with respect to other objects (e.g., spaced away from the Earth for an aircraft). Furthermore in this kind of environment what one really needs to measure is failure levels as a function frequency, amplitude, pulsewidth, direction of incidence, and polarization, since the environment is not a fixed thing but is something that can be constructed within technological limits over a wide range of design parameters.

Third, the system must be electrically configured in its operational mode. This is not a trivial requirement. Sometimes one can test an actual flying aircraft, ship at sea, etc. (although not necessarily under a full environment). Often the system is tested under other conditions, such as an aircraft on a test stand with inerted ordnance, fuel tanks, etc. Engines or some auxiliary power unit may be operated to power the electronic equipment. Under unpowered conditions there may be various switch positions that have to be rigged to preserve the electrical paths present under operational conditions.

Some might refer to this kind of test a "general's" test. This is one of its merit. The system itself is used to tell one if its performance is acceptable. One does not need to measure signal at tens of thousands of ports and process then to determine what they would have been under criteria conditions and then figure out what this would do to the system. The answer is much more. In effect the system is self-diagnosing. If one has some set of test conditions (angles of incidence, polarization directions, etc.) which reasonable cover the criterion conditions, and these are accurately reproduced in the simulation (ideally with some safety margin to allow for the errors), then the test results are as definitive as one can reasonable make them.

Test approximating this ideal have been performed in various countries, but of course the results are not usually publicized. An interesting exception is given in [169] where three systems were tested. One of these, a Swiss electric railway locomotive, was given a "complete-simulation" test (power off) in a hybrid EMP simulator; it failed. There are also some partial results concerning power distribution equipment in [147].

In the case of lightning, as discussed in Section IV, lightning simulation tests have not yet taken account of all the known important electromagnetic interaction phenomena, and as such we do not yet have a complete simulation. However, systems have often encountered the real environment. One paper [159] summarizes 877 reported lightning encounters of USAF aircraft between 1970 and 1982. Besides loss of seven aircraft, structural damage was reported in 78% of the incidents, electrical/electronic damage in 8% of the incidents. In recent years aircraft have been instrumented to measure lightning under direct-strike conditions. A NASA F-106 aircraft was instrumented for both external and internal electromagnetic response and struck hundreds of times, but with no significant damage or functional impairment [15(Pitts *et al.*, pp. 401–435), (Yang *et al.*, pp. 469–489)]. In this case the few internal current measurements gave only about one ampere (peak). A CV-580 aircraft was similarly instrumented and struck about 50 times [140], but a power supply was often damaged. A French Transall C-160 was similarly instrumented and obtained similar results [162].

D. Extrapolation

As a practical matter, no simulation is perfect. Can one quantify the errors and perhaps correct the test results to allow for some of these errors? This is the subject of extrapolation [29], [34], [37]. In this concept the system is still assumed to be operationally configured. It is the simulator environment, including the simulator/test-object interaction that is to be corrected to some degree. While one can compare the incident field at some point in the simulator to the criterion wave (by ratio of Fourier spectra) to obtain an extrapolation function, this does not allow for the inaccurate spatial variation of the incident field and for the simulator/test-object interaction.

A more general and accurate type of extrapolation uses the surface response of the system. Here we assume that the system has a highly conductive outer envelope, through which all signals must penetrate, the surface current and charge densities being the parameters that drive the penetrations. We further assume that everything from the envelope inward is operationally configured so that the transfer function from the surface to the interior "failure ports" are unchanged. Assuming the penetrations to be electrically small then define a set of surface response functions $\tilde{F}_{s_n}(s)$ for $n = 1, 2, \cdots, N$ where each n corresponds to some choice of position and either a component of the surface current density (two possible) or the surface charge density. Define a set of superscripts:

$$C \equiv \text{criterion}, \quad S \equiv \text{simulation}, \quad E \equiv \text{extrapolation}. \tag{6.1}$$

Then assume we have measured $\tilde{F}_{s_n}^{(S)}(j\omega)$ under simulation conditions, and similarly have measured (or calculated) $\tilde{F}_{s_n}^{(C)}(j\omega)$ under criteria conditions, this latter parameter often being measured using scale models [3], [26], [35], [56]. Then form the extrapolation function

$$\tilde{f}_e(j\omega) = \exp\left(\sum_{n-1}^{N} \ln\left[\frac{\tilde{F}_{s_n}^{(C)}(j\omega)}{\tilde{F}_{s_n}^{(S)}(j\omega)}\right]\right) = \left\{\prod_{n=1}^{N} \frac{\tilde{F}_{s_n}^{(C)}(j\omega)}{\tilde{F}_{s_n}^{(S)}(j\omega)}\right\}^{1/N}. \tag{6.2}$$

Here the geometric average is used, avoiding additive cancellations, although in principle one could use other types of averages.

Let $\tilde{F}_\ell(s)$ represent the (linear) response at some failure port (an internal port to some circuit of interest, etc.). Then we form the extrapolated failure-port response

$$\tilde{F}_\ell^{(E)}(j\omega) = \tilde{f}_e(j\omega)\tilde{F}_\ell^{(S)}(j\omega). \tag{6.3}$$

If we know which penetration (and surface response parameter) was driving the transfer function to the ℓth failure port then we would use just that one surface response ratio (perhaps one of the ratios in (6.2)). However, that is the point; we ostensibly do not know and the ℓth failure port is potentially any possible failure port in the system. The ratios in (6.2) are intended to sample a set of surface positions/parameters which adequately represent the variation over the test object. The extrapolation function then allows not only for deficiencies in the frequency spectrum, but also for variations in the surface field distribution from criterion conditions.

Take the surface response parameters to define a set of residual error ratios

$$\tilde{E}_{s_n}(j\omega) \equiv \frac{\tilde{F}_{s_n}^{(C)}(j\omega)}{\tilde{F}_{s_n}^{(E)}(j\omega)} \equiv \frac{\tilde{F}_{s_n}^{(C)}(j\omega)}{\tilde{f}_e(j\omega)\tilde{F}_{s_n}^{(E)}(j\omega)}. \tag{6.4}$$

These are the residual errors after extrapolation. Our extrapolated failure-port responses may be in error (high or low) by the largest and smallest of the ratios. This error represents the simulation quality in spatial sense (after correction for overall spectrum including pulser deficiencies). These errors have been measured (e.g., [34]) indicating that they can be severe (factors of 30 to 1/30) if an inappropriate simulator is used (e.g., test object parked on the ground in a hybrid simulator to simulate free flight conditions). A good simulator can have these errors a factor of two or less. So this gives us a way to measure simulation quality.

Extrapolation is useful for correcting simulator deficiencies and estimating errors, but this is not as good as complete simulation. If one is to extrapolate each failure-port signal this can apply to an enormous number of such signals. Furthermore there is the limitation of the linearity assumption. Complete simulation is defined by

$$\tilde{f}_e(j\omega) = 1, \quad \left|\tilde{E}_{s_n}(j\omega) - 1\right| \ll 1 \text{ for all } n \tag{6.5}$$

over the entire frequency range of interest. If this condition is not met one can use these concepts to raise the simulator spectrum at all frequencies (pulse amplitude) so that a design margin greater than the errors at all frequencies of interest is obtained.

E. Influence of System Design (Topology) on Ease of Testing: Penetration Tests

Suppose now that the system has been well designed with a controlled electromagnetic topology (as in Section V). Then the outermost shield has well defined localized penetrations which are all identified and small in number (say N_p). If we know the exciting parameters (full waveforms) at all the penetrations under criterion conditions (from scale models, low-level illumination of the real system, etc.) then one can construct special penetration drivers which can be operated simultaneously to achieve criterion conditions. If the penetrations are sufficiently well protected that only small signals get through, then one can use norms (as in Section V) to bound the signals inside the first shield. This in turn can be used to define penetration specifications. Some work has already been done in this direction for penetrations (windows, doors, etc.) on aircraft [6(Yang and Baum, pp. 47–59)], [105], [108]–[110], [163]–[165], [177].

Some systems are so large that they cannot be illuminated at criteria levels by a practical simulator. Consider a building with long power and communication cables extending from it. In such cases a direct drive of the penetrations, especially those associated with such conductors, becomes essential.

F. Low-Level Testing

Another kind of testing is done at very low level, say CW measurement of transfer functions from an incident field to failure ports. Sometimes low-level repetitive pulsing is similarly used. The results can be extrapolated as discussed previously [143], [176]. However, this raises the problem of linearity and the large number of potential failure ports. One use of such low-level testing might be as a prelude to a "complete simulation" for economic reasons, safety, and to gain some preliminary knowledge of anticipated system response.

In the evolution of EMP testing technology low-level testing is assuming other roles. For extended systems this is necessary to obtain the extrapolated signals for full-pulse-amplitude driving where they enter the system envelope. Furthermore, for certain purposes such as system maintenance one needs test procedures to determine proper installation and function of various items, especially penetration control devices.

G. Characterization of Failure-Port Response Parameters

When the signal reaches a failure port it can cause failure in various ways. A naive view has the energy in the pulsed signal as the only significant failure parameter. On the contrary sometimes the energy is provided by a power supply in the system, this energy dump being triggered by the transient incoming signal. More important, the signal amplitude (i.e., volts) is often the important parameter, this being associated with circuit (and perhaps functional) upset and electrical breakdown (e.g., at connectors or electronic devices). In the sense of norms (Section V) this indicates the importance of the ∞-norm (peak) and two-norm.

The electronic devices at the failure ports may well present nonlinear characteristics to the incoming signals, thereby considerably complicating our assessment problem. Of course, only a "linearity-to-failure" property is needed in which the temporal waveform encounters a linear device

(impedance characterization) for all times before device failure, after which time the linear property is not needed for our analytical purposes [90]. There are also cases in which a nonlinear element can allow bounds (particularly in two-norm sense) on response of other parts of the system based on a linear property of the rest of the system [91]. Furthermore, Section V has considered cases of special nonlinear protection devices (norm limiters) whose properties can be included in conjunction with a linear analysis.

H. Probabilistic Estimates

What one would like to have is some kind of "probability of survival" for a system in a given environment. This might allow for variation among systems of a given type, variation in environmental parameters (direction of incidence, polarization, etc.). If one had an analytical model for failure accounting for every potential failure port in the system with a probabilistic description of failure for every such port, then the model could be exercised to obtain this. However, it would be naive to assume that anything near to this exists. Experience has shown that for typical complex systems such a model cannot be practically obtained from first-principle electromagnetic calculations. The only reliable results are obtained from test in the real environment or complete simulation. To the extent that one can so test many copies of a given system in such criteria environments with variation in the environmental parameters, one can obtain such probabilistic estimates from experiment. As a practical matter a National Academy study [114] concluded: "We recommend, rather, a collection of tests, such that passing all will be acceptable as satisfaction of EMP requirements."

VII. Concluding Remarks

Looking back at my previous review in 1976 [2], it is interesting to compare the state-of-the-art then and now. Some things then in their infancy are more developed now. Some of the approaches to transient electromagnetic analysis and synthesis (as in Figs. 2 and 3 of [2]) have grown considerably with special sessions at symposia, special issues of journals, and even a book [11]. However, much research is still needed to fill out the possibilities and lead to yet more electromagnetic devices [125].

As EMP has expanded to the more general HPE technology, more applications have appeared. This process has been helped considerably by the open scientific discussion which has served as a useful filter for technical quality, and which has stimulated cross-fertilization with other areas of electromagnetics. This has served as an important modern impetus for the development of EM theory and applications.

The basic driving force for HPE technology is the potential vulnerability of electronic systems to damage and upset from exposure to the various HPE environments. While military systems have received the most attention, attention is beginning to be paid to civil systems, especially communications and power. The survivability/vulnerability of such complex electronic systems is quite variable and often unpredictable. This problem is compounded by the modern trend toward more and more sensitive electronic components.

Rigorous design and testing are required to solve the problem. Recognizing the basic commonality of system interaction with the various HPE environments, one can adopt a hardening approach which covers all these environments in a common design. The basic concept is that of electromagnetic topology involving closed surfaces, all penetrations of which are controlled (and eliminated where practical). Minimizing the number of penetrations makes testing them easier and gives fewer elements that can fail. When the system is given a "complete-simulation" (or real-environment) test one has some reason to expect that the system will pass the test. Over time one can hope that from this will evolve a set of HPE common rational specifications and standards to assure that proper techniques are used [21], [89], [92], [178]. As more common EMI/EMC problems become more severe due to proliferation of (and increasing intensities of) interfering sources, and increasing use of more and more sensitive electronics (including in more critical roles) various of these general HPE protection techniques can be usefully employed for this more general set of environments as well.

Acknowledgment

The author would like to thank the various persons who have given suggestions for improving the manuscript. He would particularly like to thank R. L. Gardner, C. L. Longmire, and W. A. Radasky for providing some of the information in Section II, concerning environments.

Bibliography

For convenience the bibliography is divided into two parts. Part I are the general references where one can find references to the earlier literature (1970's and prior). Some of these general references are compendia of papers (chapters) by various authors which are individually referenced by the main reference with a parenthetical chapter. Part II contains specific references to the more recent literature. In the interest of brevity the following abbreviations are used:

SSN	Sensor and Simulation Notes
TN	Theoretical Notes
IN	Interaction Notes
MN	Measurement Notes
SDAN	System Design and Assessment Notes
LSN	Lightning Simulation Notes
SwN	Switching Notes
CESDN	Circuit and Electromagnetic System Design Notes
MaN	Mathematics Notes

Listings of these can be found in the *IEEE Antennas and Propagation Magazine.* Copies can be requested from the author, the Defense Documentation Center, Cameron

Station, Alexandria, VA 22314, or from the Editor, Dr. Carl E. Baum, Phillips Laboratory (WSR), Kirtland AFB, NM 87117. These are also available at many universities and companies involved in electromagnetics. Where known cross reference is given to other sources.

Part I: General References, Books, Reviews, and Bibliographies

[1] E. F. Vance, Ed., Special Joint Issue on the Nuclear Electromagnetic Pulse, *IEEE Trans. Antennas Propagat.*, Jan. 1978; also in *IEEE Trans. Electromagn. Compat.*, Feb. 1978.

[2] C. E. Baum, "Emerging technology for transient and broad-band analysis and synthesis of antennas and scatterers, *Proc. IEEE*, vol. 64, pp. 1598–1616, 1976.

[3] K. S. H. Lee, Ed., *EMP Interaction: Principles, Techniques and Reference Data.* New York: Hemisphere, 1986 (from AFWL-TR-80–402, 1980).

[4] L. B. Felsen, Ed., *Transient Electromagnetic Fields.* New York: Springer-Verlag, 1976.

[5] L. W. Pearson and L. Marin, Eds., Special Issue on the Singularity Expansion Method, *Electromagnetics*, vol. 1, no. 4, 1981.

[6] W. Graf, Ed., Special Issue on Electromagnetic Topology of Large Systems, *Electromagnetics*, vol. 6, no. 1, 1986.

[7] V. Danielle and M. Ianoz, Special Issue on Electromagnetic Coupling to Transmission Lines, *Electromagnetics*, vol. 8, nos. 2–4. 1988.

[8] J. E. Thompson and L. H. Luessen, Eds., *Fast Electrical and Optical Measurements.* Dordrecht, The Netherlands: Martinus Nijhoff, 1986.

[9] E. K. Miller, Ed., *Time-Domain Measurements in Electromagnetics*, New York: Van Nostrand Reinhold, 1986.

[10] C. E. Baum, "The theory of electromagnetic interference control, IN 478, 1989; also in *Modern Radio Science 1990*, J. Bach Andersen, Ed. U.K.: Oxford University Press, 1990, pp. 87–101.

[11] C. E. Baum and A. P. Stone, *Transient Lens Synthesis: Differential Geometry in Electromagnetic Theory.* New York: Hemisphere 1991.

[12] M. A. Uman, *Lightning.* New York: McGraw Hill, 1969.

[13] R. H. Golde, *Lightning.* New York, Academic, 1977.

[14] M. A. Uman, *The Lightning Discharge.* New York: Academic, 1987.

[15] R. L. Gardner, Ed. *Lightning Electromagnetics.* New York: Hemisphere, 1990. (Includes in part: Special Issue on the Electromagnetics of Lightning, *Electromagnetics*, vol. 7, nos. 3–4, 1987.)

[16] J. C. Corbin, Ed., Special Issue on Lightning and Its Interaction with Aircraft, *IEEE Trans. Electromagn. Compat.*, May 1982.

[17] V. L. Granatstein and I. Alexeff, Eds., *High-Power Microwave Sources.* New York: Artech House, 1987.

[18] K. L. Felch, Ed., Special Issue on HIgh-Power Microwave Generation, *IEEE Trans. Plasma Sci.*, Dec. 1985.

[19] S. H. Gold and J. M. Baird, Eds., Second Special Issue on HIgh-Power Microwave Generation, *IEEE Trans. Plasma Sci.*, Apr. 1988.

[20] W. W. Destler and B. Levush, Eds., Third Special Issue on High-Power Microwave Generation, *IEEE Trans. Plasma Sci.*, June 1990.

[21] D. V. Giri, Ed., Special Issue on High-Power Microwaves, *IEEE Trans. Electromagn. Compat.*, to be published.

[22] S. Glasstone and P. J. Dolan, Eds., *The Effects of Nuclear Weapons, Third Edition.* U. S. Gov't. Printing Office, 1977.

[23] L. W. Ricketts, J. E. Bridges, and J. Miletta, *EMP Radiation and Protective Techniques,* New York: Wiley, 1976.

Part II: Specific References

[24] L. Marin, "Modes on a finite-width, parallel-plate simulator I. Narrow plates," SSN 201, 1974.

[25] T. Itoh and R. Mittra, analysis of modes in a finite-width parallel-plate waveguide, SSN 208, 1975.

[26] V. V. Liepa, "Sweep frequency surface field measurements," SSN 210, 1975.

[27] C. E. Baum, D. V. Giri, and R. D. Gonzales, "Electromagnetic field distribution of the TEM mode in a symmetrical two-parallel-plate transmission line," SSN 219, 1976.

[28] F. C. Yang and K. S. H. Lee, "Impedance of a two-conical-plate transmission line," SSN 221, 1976.

[29] C. E. Baum, "Extrapolation techniques for interpreting the results of tests in EMP simulators in terms of EMP criteria," SNN 222, 1977.

[30] L. Marin, "Modes on a finite-width, parallel-plate simulator II. Wide Plates," SSN 223, 1977.

[31] L. Marin and G. C. Lewis, Jr., "Modes on a finite-width parallel-plate Simulator III. Numerical results for modes on wide plates," SSN 227, 1977.

[32] F. C. Yang and L. Marin, "Field distributions on a two-conical-plate and a curved cylindrical-plate transmission line," SSN 229, 1977.

[33] F. C. Yang and K. S. H. Lee, "Energy confinement of a bounded-wave simulator," SSN 230, 1977.

[34] D. E. Merewether, J. F. Prewitt, and C. E. Baum, "Characterization of errors in the extrapolation of data from an EMP simulator to an EMP criterion," SSN 232, 1977.

[35] V. V. Liepa and T. B. A. Senior, "Some analysis of EC-135 aircraft model data," SSN 242, 1977.

[36] J. S. Yu, C.-L. Chen, and C. E. Baum, "Multipole radiations: Formulation and evaluation for small EMP simulators," SSN 243, 1978.

[37] C. E. Baum, "EMP simulation and its impact on EMP testing," SSN 246, 1978; also in *Proc. EMC Symp.*, Rotterdam, The Netherlands, 1979, pp. 189-194.

[38] D. V. Giri, C. E. Baum, and H. Schilling, "Electromagnetic considerations of a spatial modal filter for suppression of non-TEM modes in the transmission-line type of EMP simulators," SSN 247, 1978.

[39] V. Krichevsky and R. Mittra, "Source excitation of an open, parallel-plate waveguide," SSN 253, 1977.

[40] V. Krichevsky, "Source excitation of an open, parallel-plate waveguide, Numerical results," SSN 254, 1978.

[41] D. V. Giri, T. K. Liu, F. M. Tesche, and R. W. P. King, "Parallel plate transmission line type of EMP simulators: A systematic review and recomendations," SSN 261, 1980.

[42] F. C. Yang, "Discrete and continuous spectra of finite-width, parallel plate simulator's fields," SSN 262, 1979.

[43] J. Lam, "Excitation of the parallel-plate section of a bounded-wave EMP simulator by a conical transmission line," SSN 263, 1979.

[44] F. C. Yang, "A distributed source-region EMP simulator," SSN 266, 1980.

[45] C. E. Baum, "Sensors for measurement of intense electromagnetic pulses," SSN 271, 1981; also in *Proc. 3rd IEEE Pulsed Power Conf.*, 1981, pp. 179–185.

[46] V. V. Liepa and T. B. A. Senior, "Measured Characteristics of MGL and ACD sensors," SSN 276, 1982.

[47] C. E Baum, "Review of hybrid and equivalent-electric-dipole EMP simulators," SSN 277, 1982; also in *Proc. EMC Symp.*, Zurich, Switzerland, 1983, pp. 149–152.

[48] ——, "Idealized electric- and magnetic-field sensors based on spherical sheet impedances," SSN 283, 1983; also in *Electromagnetics*, pp. 113–146, 1989.

[49] D. V. Giri and C. E. Baum, "Airborne platform for measurement of transient or broadband CW electromagnetic fields," SSN 284, 1984; also in *Proc. AICWEMC*, Bangalore, India, 1985, pp. 79–82; also in *Electromagnetics*, pp 69–84, 1989.

[50] C. E. Baum, "Measurement of the surface curl of the current density," SSN 286, 1984; also in *Electromagnetics*, pp. 145–160, 1986.

[51] Y.-G. Chen, R. Crumley, C. E. Baum, and D. V. Giri, Field-Containing Indicators," SSN 287, 1985; also in *IEEE Trans. Electromagn. Compat.* pp. 345–350, 1988.

[52] Y.-G. Chen, R. Crumley, S. Lloyd, C. E. Baum, and D. V. Giri, "Lumped element networks for replacing sections of a buried transmission line," SSN 288, 1985; also in *IEEE Trans. Electromagn. Compat.*, 1988, pp. 449–456.

[53] C. E. Baum and D. V. Giri, "The distributed switch for launching spherical waves," SSN 289, 1985; also in *Proc. EMC Symp.*, Zurich, Switzerland, 1987, pp. 205–212.

[54] Y.-G. Chen, S. Lloyd, R. Crumley, C. E. Baum, and D. V. Giri, "Surface-current-density measurements, SSN 290, 1985; also in *Conf. Record Workshop Meas. Electrical Quantities in Pulse Power Systems II*, 1986, pp. 49–53, IEEE Dielectrics and Electrical Insulation Soc., IEEE No. 86CH2327–5.

[55] Y.-G. Chen, S. Lloyd, R. Crumley, C. E. Baum, and D. V. Giri, "Design procedures for arrays which approximate a distributed source at the air-Earth interface," SSN 292, 1986.

[56] V. V. Liepa and T. B. A. Senior, Magnetostatic surface field measurement facility," SSN 293, 1986.

[57] D. V. Giri and C. E. Baum, "Equivalent displacement for a high-voltage rollup on the edge of a conducting sheet," SSN 294, 1986; also in *Proc. INCEMIC*, Bangalore, India, 1987, pp. 229–232.

[58] G. D. Sower, "Optimization of the asymptotic conical dipole EMP sensors," SSN 295, 1986.

[59] T. M. Flanagan, C. E. Mallon, R. Denson, R. Leadon, and C. E. Baum, "A wide-bandwidth electric-field sensor for lossy media," SSN 297, 1987.
[60] C. E. Baum, "Focused aperture antennas," SSN 306, 1987.
[61] E. G. Farr, "Extrapolation of ground-alert mode data at hybrid EMP simulators," SSN 311, 1988.
[62] C. E. Baum, "Maximization of electromagnetic response at a distance," SSN 312, 1988.
[63] ——, "Coupled transmission-line model of periodic array of wave launchers," SSN 313, 1988.
[64] ——, "Some features of waveguide/horn design," SSN 314, 1988; also in *Environmental and Space Electromagnetics*, H. Kikuchi, Ed. New York: Springer-Verlag, 1991, pp. 480–497, ch. 11.3.
[65] C. Zuffada, F. C. Yang, and I. Wong, "On the thin toroidal and elliptical antennas," SSN 315, 1989.
[66] D. V. Giri, "Impendance matrix characterization of an incremental length of a periodic array of wave launchers," SSN 316, 1989.
[67] C. E. Baum, "Canonical examples for high-frequency propagation on unit cell of wave-launcher array," SSN 317, 1989.
[68] D. V. Giri, "A family of canonical examples for high frequency propagation on unit cell of wave-launcher array," SSN 318, 1989.
[69] E. G. Farr, "An incident field sensor for EMP measurements," SSN 319, 1989; also in *IEEE Trans. Electromagn. Compat.*, pp. 105–112, 1991.
[70] C. E. Baum, "Radiation of impulse-like transient fields," SSN 321, 1989.
[71] Y.-G. Chen, S. Lloyd, R. Crumley, C. E. Baum, and D. V. Giri, "Low voltage experiments concerning a section of a pulser array near the air-Earth interface," SSN 322, 1990.
[72] K. F. Casey, "The external environment of VPD-II: Space-wave field," SSN 323, 1990.
[73] ——, "The external environment of VPD-II: Ground-wave field," SSN 324, 1990.
[74] N. H. Youman and B. L. Cox, "Gigahertz analysis of the ellipticus antenna," SSN 325, 1990.
[75] D. V. Giri, "Canonical examples of high-power microwave (HPM) radiating systems for the case of one feeding waveguide," SSN 326, 1991.
[76] C. E. Baum, "Configurations of TEM feed for an IRA," SSN 327, 1991.
[77] ——, "Aperture Efficiencies for IRA's," SSN 328, 1991.
[78] E. G. Farr, "Analysis of the impulse radiating antenna," SSN 329, 1991.
[79] C. E. Baum, "General properties of antennas," SSN 330, 1991.
[80] D. V. Giri, "Efficts of waveguide dispersion on high-power microwave signals," SSN 331, 1991.
[81] C. E. Baum, W. D. Prather, and D. P. McLemore, "Topology for transmitting low-level signals from ground level to antenna excitation position in hybrid EMP simulators," SSN 331, 1991.
[82] Y. Rahmat-Samii, D. W. Duan, and D. V. Giri, "Canonical examples of reflector antennas for high power microwave applications," SSN 334, 1991.
[83] C. E. Baum, "Some considerations concerning analytic EMP criteria waveforms," TN 285, 1976.
[84] C. L. Longmire, "A nominal set of high-altitude EMP environments," TN 354, 1987, and ORNL/Sub/86-18417/1, 1987.
[85] C. L Longmire and J. L. Gilbert, "Theory of EMP coupling in the source region," TN 360, 1980, and DNA 5687F.
[86] E. F. Vance, "On electromagnetic interference control," IN 380, 1979; also in *IEEE Trans. Electromagn. Compat.*, pp. 319–328, 1980.
[87] C. E. Baum, "Electromagnetic topology: A formal approach to the analysis and design of complex electronic systems, IN 400, 1980; also in *Proc. EMC Symp.*, Zurich, Switzerland, 1981, pp. 209–214.
[88] ——, "Sublayer sets and relative shielding order in electromagnetic topology," IN 416, 1982; also in *Electromagnetics*, pp. 335–254, 1982.
[89] E. F. Vance, W. Graf, and J. E. Nanevicz, "Unification of electromagnetic specifications and standards, part I—Evaluation of existing practices," IN 420, 1981, and DNA 5433F-1.
[90] C. E. Baum, "Black box bounds," IN 429, 1983; also in *Proc. EMC Symp.*, Zurich, Switzerland, pp. 381–386, 1985.
[91] ——, "Some bounds concerning the response of linear systems with a nonlinear element," IN 438, 1984.
[92] W. Graf, J. M. Hamm, and E. F. Vance, "Unification of electromagnetic specifications and standards, part II: Recommendations for revisions of existing practices," IN 439, 1983, and DNA 5433F-1.
[93] C. E. Baum, "Effect of corona on the response of infinite-length transmission lines to infinite plane waves," IN 443, 1985; also in *Proc. EMC Symp.*, Zurich, Switzerland, 1987, pp. 321–328.
[94] ——, "On the use of electromagnetic topology for the decomposition of scattering matrices for complex physical structures," IN 454, 1985.
[95] A. H. Paxton and R. L. Gardner, "New techniques for the analysis of multiconductor transmission lines," IN 459, 1984, also as (same authors) "Application of transmission line theory to networks with a large number of component wires," in *Proc. EMC Symp.*, Zurich, Switzerland, 1987, pp. 307–312.
[96] C. E. Baum, "Transfer of norms through black boxes," IN 462, 1987; also in *Proc. EMC Symp.*, Zurich, Switzerland, 1989, pp. 157–162.
[97] ——, "High-frequency propagation on nonuniform multiconductor transmission lines in uniform media," IN 463, 1988; also in *Int. J. Numerical Modelling*, 1988, pp. 175–188.
[98] ——, "Norms of vectors of time-domain signals passing through filters and norm limiters at Subshields," IN 469, 1988; also in *Proc. EMC Symp.*, Zurich, Switzerland, pp. 589–594, 1991.
[99] ——, "Scattering, Reciprocity, symmetry, EEM, and SEM," IN 475, 1989.
[100] ——, "SEM backscattering," IN 476, 1989.
[101] J. Nitsch, C. E. Baum, and R. Sturm, "Splitting of degenerate natural frequencies in coupled two-conductor lines by distance variation," IN 477, 1989; also in *Proc. EMC Symp.*, Zurich, Switzerland. pp. 35–40, 1991.
[102] J. Nitsch, C. E. Baum, and R. Sturm, "Cummatative tubes in multiconductor-transmission-line theory," IN 480, 1990; also "Analytical treatment of circulant nonuniform multiconductor transmission lines," *IEEE Trans. Electromagn. Compat.*, pp. 28–38, 1992.
[103] J. Nitsch, C. E. Baum, and R. Sturm, "The treatment of commution nonuniform tubes in multiconductor-transmission-line theory," IN 481, 1990.
[104] C. E. Baum, "Winding topology for transformers," MN 31, 1986; also in *IEEE Trans. Electromagn. Compat.*, pp. 358–363, 1988
[105] ——, "Monitor for integrity of seams in a shield enclosure," MN 32, 1987, and *IEEE Trans. Electromagn. Compat.*, pp. 276–281, 1988.
[106] G. D. Sower and L. M. Atchley, "Twin coaxial Balun (TCB) development," MN 34, 1987.
[107] C. E. Baum, "Winding bundles for transformers," MN 35, 1987.
[108] ——, "Monitor for integrity of doors in a shield enclosure," MN 36, 1987.
[109] ——, "A spiral-transmission-line technique for detecting slot apertures in shield enclosures," MN 37, 1987.
[110] C. D. Taylor, F. Marcum, W. D. Prather, and C. C. Herrmann, "On using a sense wire to quantitate the magnetic flux leakage through an aperture in an electromagnetic shield," MN 38, 1989, and in *IEEE Trans. Electromagn. Compat.*, pp. 337–341, 1989.
[111] C. E. Baum, "An anistrotropic medium for high wave impedance," MN 39, 1991.
[112] ——, "Norm detectors for multiple signals," MN 40, 1991.
[113] ——, "Norms of time-domain functions and convolution operators," MaN 86, 1985; also in *Recent Advances in Electromagnetic Theory*, H. N. Kritikos and D. L. Jaggard, Eds. New York: Springer-Verlag, 1990, pp. 31–55, ch. 2.
[114] Committee on Electromagnetic Pulse Environment, Evaluation of Mehtodologies for Estimating Vulnerability to Electromagnetic Pulse Effects, SDAN 27, 1984, and National Academy Press, 1984.
[115] C. N. Vittitoe, "Did high-altitude EMP cause the Hawaiian streetlight incident," SDAN 31, 1989.
[116] C. E. Baum, "Simulation of electromagnetic aspects of lightning," LSN 1, 1980; also in *Environmental and Space Electromagnetics*, H. Kikuchi, Ed. New York: Springer-Verlag, 1991, pp. 463–479, ch. 11.2.
[117] I. Smith, "Breakdown of uniform field pressurized SF_6 spark gaps as a function of charge time," SwN 27, 1987.
[118] J. L. Harrison, "Solution of peaking equation for finite storage capacitor size," CESDN 32, 1973.
[119] D. V. Giri and C. E. Baum, "Theoretical considerations for optimal positioning of peaking capacitor arms about a Marx generator parallel to a ground plane," CESDN 33; also in *Proc. INCEMIC*, Bangalore, India, 1987, pp. 43–46; also in *IEEE Trans. Electomagn. Compat.*, 1989, pp. 117–124.
[120] ——, "Optimal positioning of a set of peaker arms in a ground plane," CESDN 35, 1988.

[121] D. V. Giri and C. E. Baum, "Coupled transmission-line model of Marx generator with peaking-capacitor arms," CESDN 36, 1988.
[122] C. E. Baum, "Combining RF sources using C_N symmetry," CESDN 27, 1989.
[123] C. E. Baum, "Matching modulated electron beam to waveguide," CESDN 39, 1990.
[124] D. V. Giri, "Preliminary considerations for high-power microwave (HPM) radiating systems," CESDN 40, 1990.
[125] C. E. Baum and H. N. Kritikos, "Symmetry in electromagnetics," Physics Note 2, 1990.
[126] M. Krook, R. W. P. King, D. J. Blejer, T. K. Sarkar, and S.-K. Wan, "The electric field in a model parallel-plate EMP simulator at a high CW frequency," Miscellaneous Simulator Memo 17, 1978.
[127] J. C. Giles, M. K. Baumgardner, G. Seely, and J. Furaus, "Evaluation and improvement of the CW performance of the ALECS facility," ALECS Memo 10, 1975.
[128] S. Garmland, "Electromagnetic characteristics of the conical transmission-line EMP simulator SAPIENS," SAPIENS Memo 11, 1986.
[129] D. V. Giri, "Terminator design for SAPIENS-II," SAPIENS Memo 12, 1990.
[130] C. E. Baum, J. P. O'Neill, G. D. Sower, E. L. Breen, I. J. Caylor, D. L. Hall, and C. B. Moore, "Kiva 2 lightning current measuring sensor array," Kiva Memo 4, 1984.
[131] J. R. Legro, N. C. Abi-Samra, and F. M. Tesche, "Study to assess the effects of magnetohydrodynamic electromagnetic pulse on electric power systems," Phase I Final Report, ORNL/Sub-83/43374/1/V3, 1985.
[132] R. W. P. King and D. J. Blejer, "The electromagnetic field in an EMP simulator at a high frequency," *IEEE Trans. Electromagn. Compat.*, pp. 263–269, 1979.
[133] H. Trinks, G. Matz, and H. Schilling, "Electro-Optical system for EMP measurement," *IEEE Trans. Electromagn. Compat.*, pp. 75–77, 1980.
[134] R. W. P. King, D. J. Blejer, and T. T. Wu, "Standing waves and notches in an EMP simulator and their reduction," *IEEE Trans. Electromagn. Compat.*, pp. 80–87, 1981.
[135] H.-M. Shen and R. W. P. King, "The rhombic EMP simulator," *IEEE Trans. Electromagn. Compat.*, pp. 255–265, 1982.
[136] H.-M. Shen and R. W. P. King, "Experimental investigation of the rhombic EMP simulator: comparison with theory and parallel-plate simulator," *IEEE Trans. Electromagn. Compat.*, pp. 349–355, 1982.
[137] M. A. Uman, M. J. Master, and E. P. Krider, "A comparison of lightning electromagnetic fields with the nuclear electromagnetic pulse in the frequency range 10^4–10^7 Hz," *IEEE Trans. Electromagn.*, pp. 410–416, 1982.
[138] W. J. Broad, "The chaos factor," *Science 83*, pp. 40–49, Jan./Feb. 1983.
[139] M. Kanda, "Time domain sensors for radiated impulsive measurements," *IEEE Trans. Antennas Propagat.*, pp. 438–444, 1983.
[140] P. L. Rustan, "Description of an aircraft lightning and simulated nuclear electromagnetic pulse (NEMP) threat based on experimental data," *IEEE Trans. Electromagn. Compat.*, pp. 49–63, 1987.
[141] C. Zuffanda and N. Engheta, "Field uniformity criteria for the design of a two-wire EMP simulator," *Electromagnetics*, pp. 29–35, 1988.
[142] E. F. Vance and M. A. Uman, "Differences between lightning and nuclear electromagnetic pulse interactions," *IEEE Trans. Electromagn. Compat.*, pp. 54–62, 1988.
[143] F. M. Tesche and P. R. Barnes, "Extrapolation of measured power system response data to high-altitude EMP excitation," *IEEE Trans. Electromagn. Compat.*, pp. 386–392, 1988.
[144] J. E. Nanevicz, E. F. Vance, W. Radasky, M. A. Uman, G. K. Soper, and J. M. Pierre, "EMP susceptibility insights from aircraft exposure to lightning," *IEEE Trans. Electromagn. Compat.*, pp. 463–472, 1988.
[145] C. E. Baum, "A career (to date) in electromagnetics," *IEEE Antennas Propagat. Newsletter/Mag.*, pp. 12–17, December 1989.
[146] H.-M. Shen, R. W. P. King, and T. T. Wu, "New sensors for measuring very short electromagnetic pulses," *IEEE Trans. Antennas Propagat.*, pp. 838–846, 1990.
[147] F. M. Tesche and P. R. Barnes, "Transient response of a distribution circuit recloser and control unit to a high-altitude electromagnetic pulse (HEMP) and lightning," *IEEE Trans. Electromagn. Compat.*, pp. 113–124, 1990.
[148] J. R. Wait and P. Teschan, "Basic limitation in interpreting field waveforms of lightning return strokes at a distant point," *IEEE Trans. Electromagn. Compat.*, pp. 249–250, 1990.
[149] J. LoVetri and G. I. Costache, "An electromagnetic interaction modeling advisor," *IEEE Trans. Electromagn. Compat.*, pp. 241–251, 1991.
[150] J. P. Parmantier, G. Labaune, J. C. Alliot, and P. Degauque, "Electromagnetic coupling on complex systems: Topological approach," *LaRecherche Aérospatial*, no. 5, pp. 57–70, Sept.-Oct. 1990.
[151] J. P. Parmantier, G. Labaune, J. C. Alliot, and P. Degauque, "Electromagnetic topology: Junction characterization methods," *La Recherche Aérospatial*, no. 5, pp. 71–82, Sept.-Oct., 1990.
[152] C. Leteinturier, C. Weidman, and J. Hamelin, "Current and electric field derivatives in tiggered lightning return strokes," *J. Geophysical Research*, vol. 95, no. D1, pp. 811–828, 1990.
[153] C. E. Baum, E. J. Rothwell, K. M. Chen, and D. P. Nyquist, "The singularity expansion method and its application to target identification," *Proc. IEEE*, pp. 1481–1492, 1991.
[154] P. A. A. Sevat, "A fibre optic link for EMP measurements," in *Proc. EMC Symp.*, Rotterdam, The Netherlands, 1979, pp. 215–218.
[155] G. Sower, "I-Dot Probes for pulsed power monitors," in *Proc. 3rd IEEE Int. Pulsed Power Conf.*, 1981, pp. 189–192.
[156] G. D. Sower, A. J. Bonham, M. E. Gruchalla, and J. R. Pressley, "Instrumentation for EMP Measurements," *Proc. EMC Symp.*, Zurich, Switzerland, 1983, pp. 65–70.
[157] D. V. Giri, "Review of guided wave EMP simulators," *Proc. EMC Symp.*, Zurich, Switzerland, 1983, pp. 153–156.
[158] I. D. Smith, "The pulse power technology of high altitude EMP simulators," *Proc. EMC Symp.*, Zurich, Switzerland, 1983, pp. 157–162.
[159] J. C. Corbin, "Lightning interaction with USAF aircraft," in *Proc. 8th Int. Aerospace and Ground Conf. Lightning and Static Electricity*, Fort Worth, TX, 1983, pp. 66–1 through 66–6.
[160] J. C. Giles, "A survey of simulators of EMP outside the source region: Some characteristics and limitations," NEM 1984, Baltimore, MD (revised May 1985, EG&G Document).
[161] P. L. Rustan, Jr. and J. P. Moreau, "Aircraft lightning attachment at low altitudes," in *Proc. 10th Int. Aerospace and Ground Conf. Lightning and Static Electricity*, Paris, France, 1985, pp. 259–265.
[162] J. P. Moreau and J. C. Alliot, "E and H fields measurements on the Transall C160 Aircraft during lightning flashes," *Proc. 10th Int. Aerospace and Ground Conf. Lightning and Static Electricity*, Paris, France, 1985, pp. 281–287.
[163] L. O. Hoeft, C. M. Graves, P. J. Miller, and W. D. Prather, "Development of a cable shield tester for *in-situ* hardness surveillance of cables," *Proc. IEEE Int. Symp. EMC*, 1987, pp. 67–71.
[164] J. Beilfuss, J. Capobianco, and R. Gray, "EMP simulation for hardness verification testing," in *Proc. IEEE Int. Symp. EMC*, 1987, pp. 139–147.
[165] L. O. Hoeft, C. Herrmann, and W. D. Prather, "Measured electromagnetic performance of hardening elements for aircraft windows and doors," in *Proc. IEEE Int. Symp. EMC*, 1987, pp. 168–171.
[166] R. L. Gardner, "High power electromagnetics: A generalization of EMP technology," in *Proc. EMC Symp.*, Zurich, Switzerland, 1989, pp. 153–156.
[167] K. Madsen, "Extrapolation of transient EMP data, using Prony's method for pole-extraction in the time domain," in *Proc. EMC Symp.*, Zurich, Switzerland, 1989, pp. 169–174.
[168] J. L. Gilbert and C. L. Longmire, "Surface burst EMP environments and coupling," *Proc. EMC Symp.*, Zurich, Switzerland, 1989, pp. 175–178.
[169] D. Hansen, H. Schaer, D. Koenigstein, H. Garbe, and H. Hoitink, "A methodology to assess ExoNEMP impact on a real system—Case studies," in *Proc. EMC Symp.*, Zurich, Switzerland, pp. 185–190, 1989.
[170] F. M. Tesche, "On the reconstruction of a transient waveform from spectral magnitude data," *Proc. EMC Symp.*, Zurich, Switzerland, 1989, pp. 191–196.
[171] C. Leteinturier, J. Hamelin, and C. Weidman, "Correlation of lightning current and electric field derivative," *Proc. EMC Symp.*, Zurich, Switzerland, 1989, pp. 405–410.
[172] J. LoVetri, S. Abu-Hakima, A. S. Podgorski, and G. I. Costache, "HardSys: Applying expert system techniques to electromagnetic hardening," in *Proc. 1989 IEEE Symp. EMC*, pp. 383–385.
[173] W. A. Radasky, "Review of unclassified HEMP calculations and analytic waveforms," *NEM 1990 Record*, p. 71.
[174] H. E. King and J. L. Wong, "Measured RF characteristics of a TEM-wire fed reflector," *IEEE 1990 Antennas Propagat. Symp. Digest*, pp. 266–269.
[175] D. V. Giri, J. Fang, P. Mani, and M. Nyffeler, "Near fields of an impedance-loaded elliptical antenna," in *Proc. EMC Symp.*, Zurich,

Switzerland, 1991, pp. 363–366.
[176] T. Karlsson and F. M. Tesche, "CW Test concepts for HEMP hardness validation: Overview and test results for an unhardened telephone switching facility," *Proc. EMC Symp.*, Zurich, Switzerland, 1991, pp. 373–376.
[177] J. P. Parmantier and J. P. Aparicio, "Electromagnetic topology: Coupling of two wires through an aperture," *Proc. EMC Symp.*, Zurich, Switzerland, 1991, pp. 595–600.
[178] MIL-STD-188–125, "High-altitude Electromagnetic Pulse (HEMP) Protection for Ground-Based C^4| Facilities Performing Critical, Time-Urgent Missions," 1990.
[179] J. D. Jackson, *Classical Electrodynamics, 2nd Edition.* New York: Wiley, 1975.
[180] C. E. Baum, "The role of scattering theory in electromagnetic interference problems," in *Electromagnetic Scattering,* P.L.E. Uslenghi, Ed. New York: Academic, 1978, pp. 471–502.
[181] ——, "Toward an engineering theory of electromagnetic scattering: The singularity and eigenmode expansion methods," in *Electromagnetic Scattering,* P.L.E. Uslenghi, Ed. New York: Academic, 1978, pp. 571–651.
[182] R. Breuer and H. Lechleitner, *Der Lautlose Schlag.,* Munich, Germany: Meyster Verlag, 1982.
[183] C. H. Lee, *Picosecond Optoelectronic Devices.* New York: Academic, 1984.
[184] J. Chew, *Storms Above the Desert.* Albuquerque, NM: Univ. of New Mexico Press, 1987.
[185] Y. Rahmat Samii, Reflector Antennas, *Antenna Handbook,* Y. T. Lo and S. W. Lee, Eds. New York: Van Nostrand Reinhold, 1988, ch. 15.
[186] M. Weiner and K. H. Schoenbach Eds., Special Issue on the Optical and Electron-Beam Control of Semiconductor Switches, *IEEE Trans. Electron Dev.,* Dec. 1990.
[187] H. Lechleitner and H. Breuer, "Bilder aus der Wisenschaft," Broadcast 30, Sept. 1981, 2145 hours, Munich, Germany.
[188] P. L. Rustan, private communication.

Carl E. Baum (Fellow, IEEE) was born in Binghamton, New York, on February 6, 1940. He received the B.S. (with honor), M.S., and Ph.D. degrees in electrical engineering from the California Institute of Technology, Pasadena, in 1962, 1963, and 1969, respectively.

He was commissioned in the United States Air Force in 1962 and was stationed at the Phillips Laboratory (formerly Air Force Weapons Laboratory) from 1963 to 1967 and from 1968 to 1971. Since 1971 has served as a Civil Servant with a position as Senior Scientist at the Phillips Laboratory. He has co-authored a book, *Transient Lens Synthesis: Differential Geometry in Electromagnetic Theory.*

Dr. Baum has been awarded the Air Force Research and Development Award (1970) and the AFSC Harold Brown Award (1990). He is editor of several interagency note series on EMP (electromagnetic pulse) and related subjects and has received the Richard R. Stoddart award of the IEEE EMC Society. He is recipient of the 1987 Harry Diamond Memorial Award with citation: "for outstanding Contributions to the knowledge of transient phenomena in electromagnetics." He is a member of Commissions B & E of the U.S. National Committee of the International Union of Radio Science (URSI). He is founder and president of SUMMA Foundation which sponsors various electromagnetics related activities including scientific conferences, publications, short courses, and awards. He has led an EMP short course at numerous locations around the globe.